NASA-CR-199333

65169
p. 57

Advances in Hypersonic Vehicle Synthesis with Application to Studies of Advanced Thermal Protection Systems

Final Report

Dr. Mark D. Ardema
Principal Investigator

N96-10793
Unclas
G3/18 0065169

(NASA-CR-199333) ADVANCES IN HYPERSONIC VEHICLE SYNTHESIS WITH APPLICATION TO STUDIES OF ADVANCED THERMAL PROTECTION SYSTEM Final Report, 15 Jun. 1994 - 30 Sep. 1995 (Santa Clara Univ.) 57 p

June 15, 1994 - September 30, 1995

Santa Clara University
Santa Clara, CA 95053

NASA Ames Research Center Grant NCC2-5069

Introduction

This report summarizes work accomplished under NASA Grant NCC2-5069, June 15, 1994 to September 30, 1995, entitled "Advances in Hypersonic Vehicle Synthesis with Application to Studies of Advanced Thermal Protection Systems." The effort was in two areas: (1) development of advanced methods of trajectory and propulsion system optimization, and (2) development of advanced methods of structural weight estimation. The majority of the effort was spent in the trajectory area. During the course of the grant, there were slight deviations from the original work statement due to changing priorities of the sponsor. H.-C. Chou and M. Chambers were the graduate student research assistants assigned to the project.

Review of Results in Trajectory and Propulsion System Optimization

(1) An initial period was spent on a critical review of the trajectory optimization routines in HAVOC (Hypersonic Air Vehicle Optimization Code). This was necessary to enable the student graduate research assistant to become familiar with the code. In the process, the code was somewhat streamlined and some minor errors were corrected.

(2) A previously developed method of trajectory optimization (Refs. 1 and 2) was extended to enable computation of near-optimal trajectories for minimum fuel mass, minimum fuel volume, minimum time, minimum heat load, or a weighted combination of these. The method is based on energy-state approximation and provides a guidance algorithm that rapidly computes near-optimal trajectories as an integral part of the trajectory routine in HAVOC. The algorithm also determines key propulsion system operation parameters, such as throttle switching between multiple propulsion modes.

Figures 1 and 2 illustrate the results from the guidance algorithm. Displayed are minimum fuel weight, fuel volume, time, and heat load trajectories for the ascent of a single-state-to-orbit (SSTO) vehicle with both an airbreathing and a rocket engine. The minimum and maximum dynamic pressure limits were 200 and 2000 psf, respectively.

Figure 1 shows that the minimum weight trajectory generally follows a maximum dynamic pressure (q max) boundary, except for a transonic dive and at high hypersonic speeds. Figure 2 shows that the rocket is off except for an initial boost below M1 and that the airbreather is always on full.

The minimum fuel volume case has the rocket on full, except for a brief period from M17 to M19, when it is off. This is to be expected because the rocket propellant has relatively high density. While the rocket is on, the trajectory in the hypersonic range is at relatively low q.

Both the minimum time and minimum heat trajectories are at q max and both propulsion system modes are fully on for the entire ascent (although the minimum time trajectory results in minimum heat input, it may be that surface temperature limits are exceeded along this trajectory

for some thermal protection systems.) The vehicle weight histories along the trajectories are shown on Figure 3. All trajectories start with a gross lift-off weight of 317,000 lbs. The minimum time and minimum heat load ascent trajectories end at 10 min. with a vehicle weight of 110,000 lbs, the minimum fuel volume trajectory at 17 min. with 100,000 lbs., and the minimum fuel weight trajectory at 25 min. and 145,000 lbs. Thus, there is a significant difference in time and fuel consumed between these trajectories.

(3) A study was done of optimizing operation of the propulsion systems of SSTO airbreathing/rocket vehicles. The results were presented as AIAA Paper No. 94-3635 at the AIAA Guidance, Navigation, and Control Conference, August 1-3, 1994, Scottsdale, Arizona, entitled "Near Optimal Propulsion System Operation for Air-Breathing Launch Vehicles." The paper has also been accepted for publication in the *Journal of Spacecraft and Rockets*. This paper is attached as Appendix A and will be only briefly reviewed here.

A cost functional based on energy--state approximation was used to optimize propulsion system operation of a single-stage-to-orbit hybrid air-breathing launch vehicle. The first issue addressed was optimal throttle switching of rocket and airbreathing engine modes. It was found that in most cases the airbreathing mode was at full throttle for the entire ascent trajectory, and the rocket was off until a high hypersonic speed, and then on full for the rest of the trajectory.

The use of liquid oxygen (LOX) augmentation in the scramjet engine was also considered. It was found that LOX augmentation is optimal at high hypersonic speeds, but this conclusion is sensitive to scramjet engine modeling. It was also determined that it is far better to carry the LOX from take-off rather than collecting and separating air during flight.

(4) Decent trajectories for airbreather/rockets were also investigated. Figure 4 shows the ascent (solid line) and descent (dashed) trajectories as determined by the energy-state method for minimum time. The trajectories for minimum heating (Figure 5) are very similar to those for minimum time.

(5) The next task accomplished was a study of descent trajectories with heating and temperature constraints for a SSTO rocket. Figure 6 shows that if no temperature constraints are imposed, the minimum heat load trajectory is also the minimum time trajectory, and follows a q max (900 psf) boundary. Figure 7 shows the cost functional (Ps/B) as a function of altitude and Mach number. It is seen that there is another local optimum at very low q.

The temperatures at various points on the vehicle (PBT = distance from nose/vehicle length) as a function of M are shown on Figure 8. Many of these temperatures are higher than allowable for the preferred thermal protection system, and thus temperature limits must be imposed on the trajectory. Figure 9 shows temperature profiles in the flight envelope for PBT = 0.25. Maximum temperatures at this point on the body are 800°F for the upper surface (TUS) and 1800°F for the lower surface (TLS). Following these paths is not possible because the change in q along them is not monotonic. The procedure followed is to first search for the lowest

q along the constant limit temperature paths and then begin the trajectory at this q. When the temperature limit path is reached, it is then followed until the q max boundary is reached. The resulting trajectory is shown in Figure 10.

(6) The final work in the trajectory area was a study of the optimal operation of dual-fuel SSTO rockets. A paper giving the results has been submitted to the *Journal of Spacecraft and Rockets*. This paper is attached as Appendix B and will be only briefly reviewed here.

A simple guidance law for operation of dual-fuel SSTO launch vehicles was developed and used to determine the optimal value of the transition Mach number from dual-fuel to single-fuel. for the example considered, the optimal transition Mach number was 9.0 along a fixed trajectory. Along an optimal trajectory, the best transition Mach number was 9.6; the optimal trajectory had higher dynamic pressure than the fixed, particularly in dual-fuel mode.

In the future, the guidance method described in this paper easily could be extended to optimize other propulsion system parameters, such as flow rates of individual propellants in multi-propellant engines. In addition to being a useful tool for preliminary design studies, the guidance law could be used for real-time on-board control of SSTO launch vehicles.

Review of Results in Structural Analysis and Weight Estimation

(1) The ability to size the body structure to meet strain limits was developed. This is important for thermal protection systems with relatively rigid materials which are attached to the structure. This has been added to the existing structural weight routines (Refs. 3-5) and is now operational in HAVOC.

(2) A new structural concept has been added to the library of concepts in HAVOC. The new concept consists of a Z-stiffened shell with frames, and is sized to put most of the structural material in the skin. This gives a structure with poor buckling efficiency but is relatively light when pressure loads in integral tanks are dominant.

(3) The ability to specify frame spacing was added to HAVOC (previously, frame spacing was computed internally to minimize total weight of the shell and frames). This is important because it allows thermal protection system panels of fixed dimensions to be attached to the frames at their edges.

A vehicle was chosen for an analysis with specified values of frame spacing set constant along the length of the body. Comparisons were made with this vehicle's optimized unit weights and optimized frame spacing. Within the midbody of the vehicle, the optimized spacing stayed constant at 39.8 inches. Figure 11 shows the variation of unit weights for the vehicle as functions of specified frame spacing. Minimum total weight was achieved at a frame spacing of approximately 40 inches, giving good agreement with the optimized vehicle. It is seen that body weight rises rapidly as frame spacing is decreased to very low values. Unit weights were also

similar to the optimized results. It should be noted that frame spacing may be independently set along each body segment (witn a maximum of 12 segments) to more closely match a given design.

(4) An analysis incorporating the static head pressure in the design loads was undertaken. This is important for vertical take-off SSTO's which have large propellant tanks.

(5) An analysis of multiple element body structures was completed. This will allow estimation of structural weight of bodies which have load sharing between two discrete elements, such as a tank and an external shell. Three separate loading cases have been investigated concerning the structural behavior of a two-element composite, thin-walled beam. The first case examines the effect of bending stress in the beam. The second and third involve axial and hoop pressure stresses. Due to changing priorities, this analysis has not been implemented in HAVOC.

We first investigated the bending stress due to an externally applied longitudinal bending moment of magnitude M in a two-element, composite, thin-walled beam. A general model of this beam is shown in Figure 12. The neutral axis is found using the technique of Timoshenko and Gere from Equation (5-32) in Reference 6. (A sign change will be made, so that y and r are always positive, representing only magnitudes of distances). The neutral axis will lie on the line about which the resultant axial force acting on the two elements is equal. The axial force as a function of distance y from the neutral axis for each element is

$$\int_i \sigma_{x_i} dA = E_i \int_i y dA$$

where σ_{x_i} is the axial stress on a differential area of the element, and E is Young's modulus of elasticity. Equating the two axial forces

$$E_1 \int_1 y dA = E_2 \int_2 y dA$$

where y is measured as a positive value from this neutral axis. The axial force on each element, which may be expressed as a function of the distance of the centroid of each element from the neutral axis, r_i, is

$$\int_i y dA = r_i P_i t_i$$

where P_i and t_i are the perimeter and thickness of each element. Solving for r_i in terms of some reference axis, x′, shown on Figure 12, gives

$$r_2 = \frac{c_2 - c_1}{1 + \frac{E_1 P_2 t_2}{E_2 P_2 t_2}}$$

$$r_1 = c_2 - r_2 - c_1$$

$$\bar{c} = c_1 + r_1$$

The bending stress is found using Equation (5-34) from Reference 6. The maximum axial unit loads are found to be

$$N_1 = \sigma_1 t_1$$
$$= \frac{Mb_1 E_1 t_1}{E_1 I_1 + E_2 I_2}$$

$$N_2 = \sigma_2 t_2$$
$$= \frac{Mb_2 E_2 t_2}{E_1 I_1 + E_2 I_2}$$

where M is the applied moment, I_i is the moment of inertial of each element, and the extreme fiber distances, b_1 and b_2, are set equal to

$$b_1 = \max(r_1 + b_{d_1}, |r_1 - b_{u_1}|)$$
$$b_2 = \max(r_2 + b_{u_2}, |r_2 - b_{d_2}|)$$

respectively. The area moments of inertia about the structural neutral axis are found to be

$$I_1 = I_1' t_1 + P_1 t_1 r_1^2$$

$$I_2 = I_2' t_2 + P_2 t_2 r_2^2$$

where I_i' is the unit moment of inertia of each element. Substituting these inertias into the unit loads and simplifying, we obtain

$$N_1 = \frac{Mb_1}{I_1' + P_1 r_1^2 + \frac{E_2 t_2}{E_1 t_1}(I_2' + P_2 r_2^2)}$$

$$N_2 = \frac{Mb_2}{\frac{I_1' + P_1 r_1^2}{\frac{E_2 t_2}{E_1 t_1}} + I_2' + P_2 r_2^2}$$

Note that each unit load is a function of the ratio of the equivalent isotropic wall thicknesses. Thus, the equations are coupled, and an iterative procedure must be used to solve for the thicknesses to give the least weight structure. A method is suggested as follows:

(1) Guess (t_2/t_1)
(2) Compute N_1, N_2
(3) Compute t_1, t_2
(4) Compute (t_2/t_1)
(5) Compute new estimate of (t_2/t_1) (using algorithm below)
(6) Go to (2)

Possible algorithms:
(1) Newton iteration to drive error to zero
(2) Piccard iteration

The hoop stress interaction between two concentric, thin-walled cylindrical shells, where the inner shell is under internal pressure, was investigated. The inner shell, assumed to be a tank, carries an internal pressure of 15 psi, or atmospheric pressure. The outer shell, connected in some fashion to the inner shell by discrete elements, will share some portion of the inner shell's hoop load. We wish to find the amount of load, and hence stress, that is distributed from the inner to the outer shell. This distribution will depend upon the diameters and thicknesses of the shells; the material properties of the shells; and the placement, number, and degree of rigidity of the elements used to separate the shells.

A simple model of a small portion of a cylinder was constructed. This small arc-length model was first analyzed by hand, and then by the finite element method using the NASTRAN computer program. A small portion of a unit-length of cylinder under internal pressure, p, is shown in Figure 13. Using a free-body diagram of the internal pressure and reactive forces on this element, the hoop stress may be found as follows: Assuming small angles, the internal pressure may be replaced with a force P_i which acts at the center of the element. For a unit-length along the shell, P_i is equal to

$$P_i = pr_i\theta$$

$$\theta \approx 0.$$

where θ is measured about the axis of revolution of the cylinder. Summing forces in the radial direction, the hoop stress R_i is found to be

$$\sum F_r = 0. = P_i - R_i\theta$$

$$R_i = pr_i$$

The magnitude of R_i matches the hoop load for a thin-walled cylinder under internal pressure p.

Next we create a model of a small portion of two concentric cylindrical shells. A 14-element finite element model was constructed to analyze this hoop stress interaction. Three shell elements were used for both the inner and outer shell structures, in addition to 8 axial elements to connect the corners of the shell elements. The dimensions of the shell elements is 10 inches by approximately 12 inches. A diagram of this finite element model is shown in Figure 14. Two types of connection between the inner and outer shells was investigated. For one case, the axial elements were rods which had specified cross-sectional areas and the same material properties as the shell elements. A plot of shell and axial rod stresses is shown in Figure 15 for this configuration. In the other case, the axial elements were linear springs with specified spring constants. A plot of shell stresses is shown in Figure 16 for this configuration. Material is assumed to be high strength aluminum, with a shell wall thickness of 0.02 inch.

The final activity concerning composite shells was an analysis of the effect of internal axial pressure on a composite structure of two concentric, thin-walled cylindrical shells, where the inner shell is under internal pressure. Figure 17 shows the unpressurized structure, and the limit load cases, where the load sharing between the inner and outer cylinders is either negligible or complete. A trivial solution exists when the outer structure shares no load. In the case of complete load sharing, the axial load will be transferred between the inner and outer cylinders through some kind of shear wall, as yet unspecified. Thus, the axial deflection, δ, and axial strain, ε, must be the same for the two cylinders

$$\varepsilon_c = \varepsilon_1 = \varepsilon_2$$
$$\delta_1 = L\varepsilon_1$$
$$\delta_2 = L\varepsilon_2$$
$$\delta_c = L\varepsilon_c$$

where L is the length of the structure. But it is not true that the axial stresses in the two cylinders are the same. The axial force caused by pressure inside the inner cylinder is

$$F_p = pA_1 = \pi p r_1^2$$

where A_1 and r_1 are the cross-sectional area and radius of the inner cylinder. This axial force will be resisted by both the inner and outer cylinders by forces F_{p_1} and F_{p_2} respectively, such that $F_p = F_{p_1} + F_{p_2}$. The axial deflection of the inner and outer cylinders is

$$\delta_1 = \frac{F_{p_1} L}{A_1 E_1}$$

$$\delta_2 = \frac{F_{p_2} L}{A_2 E_2}$$

respectively. Setting these deflections equal to one another, and solving for F_{p_1} and F_{p_2}, gives

$$F_{p_1} = \frac{p r_1^2 \pi}{1 + \frac{A_2 E_2}{A_1 E_1}}$$

$$F_{p_2} = \frac{p r_1^2 \pi}{1 + \frac{A_1 E_1}{A_2 E_2}}$$

Two checks may be made for these formulas for trivial cases. The first is for two cylinders of similar cross-sectional areas and material properties. This results in one-half the deflection of a single cylinder. The second is for an outer cylinder of no cross-sectional area (or, conversely, of negligible elasticity). This results in the correct deflection of a single cylinder.

Two observations have been made regarding these results. The first is that a relatively thick, and heavy, rigid support must be provided to allow the outer shell to relieve appreciable hoop stress from the inner shell. The second is that a similarly high spring constant must be used for the elastic supports to achieve the same relief. There is also the concern that high local stresses will be created in the thin shells through the discrete supports. No investigation was made into the effect of this stress concentration.

References

1. Ardema, M. D., Bowles, J. V., and Whittaker, T., "Optimal Trajectories for Hypersonic Launch Vehicles," *Dynamics and Control*, 4, 1994, pp. 337-347.

2. Ardema, M. D., Bowles, J. V., Terjesen, E. J., and Whittaker, T., "Approximate Altitude Transitions for High-Speed Aircraft," *Journal of Guidance, control, and Dynamics*, Vol. 18, No. 3, May-June 1995, pp. 561-566.

3. Ardema, M.D.: Body Weight of Hypersonic Aircraft: Part 1, NASA TM-101028, Oct. 1988.

4. Ardema, M. D.; and Chambers, M. C.: Body Weight of Hypersonic Aircraft: Part 2. NASA TM-102797, Aug. 1990.

5. Ardema, M.D.; Chambers, M.C.; Terjesen, E.; and Roberts, C.: Body Weight of Advanced Concept Hypersonic Aircraft: NASA TM-103893.

6. Timoshenko, S.P.; and Gere, J. M.: *Mechanics of Materials*, Van Nostrand Reinhold, 1972

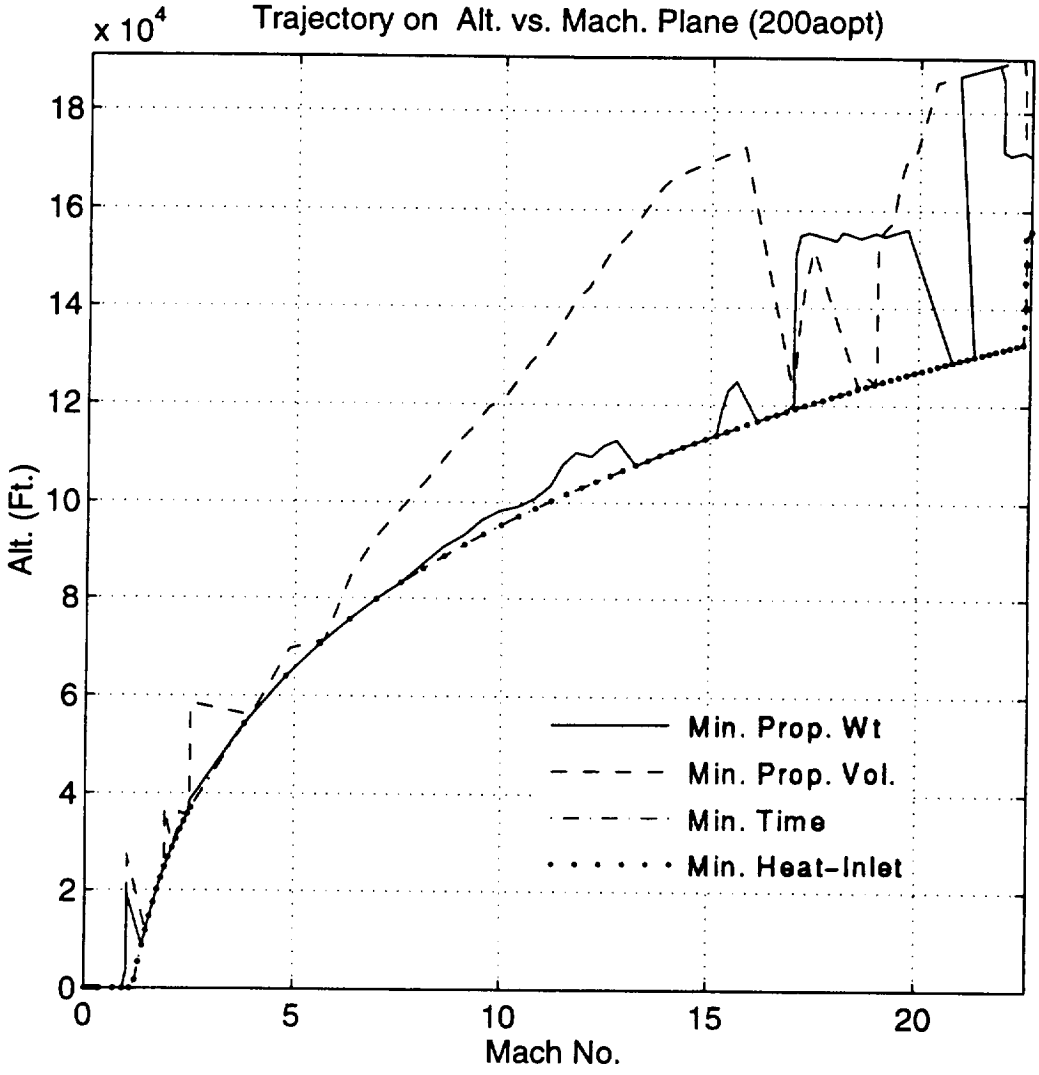

Figure 1. The optimized flight paths of ABLV.

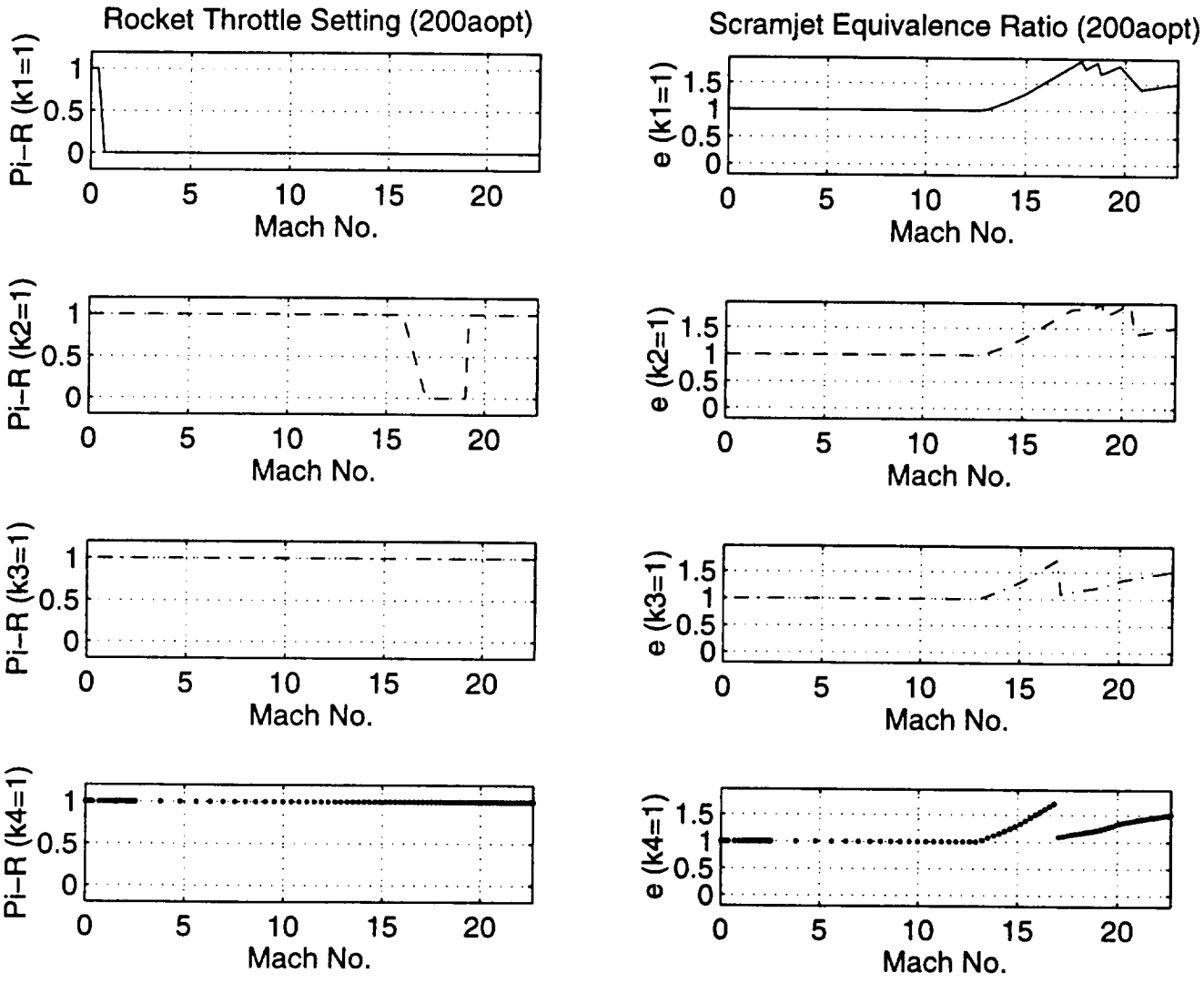

Figure 2. Optimal throttle schedules of ABLV.

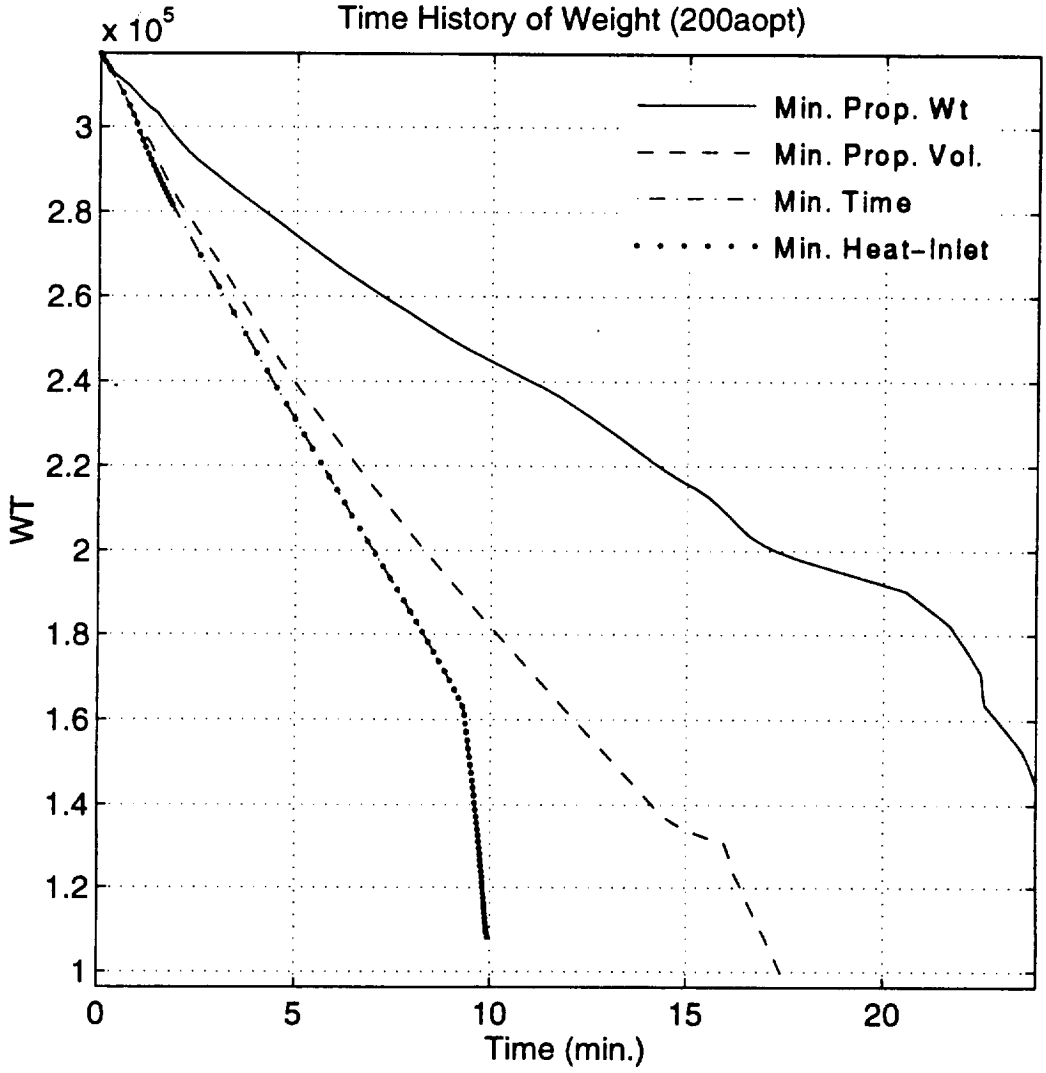

Figure 3. Time histories of weights of ABLV.

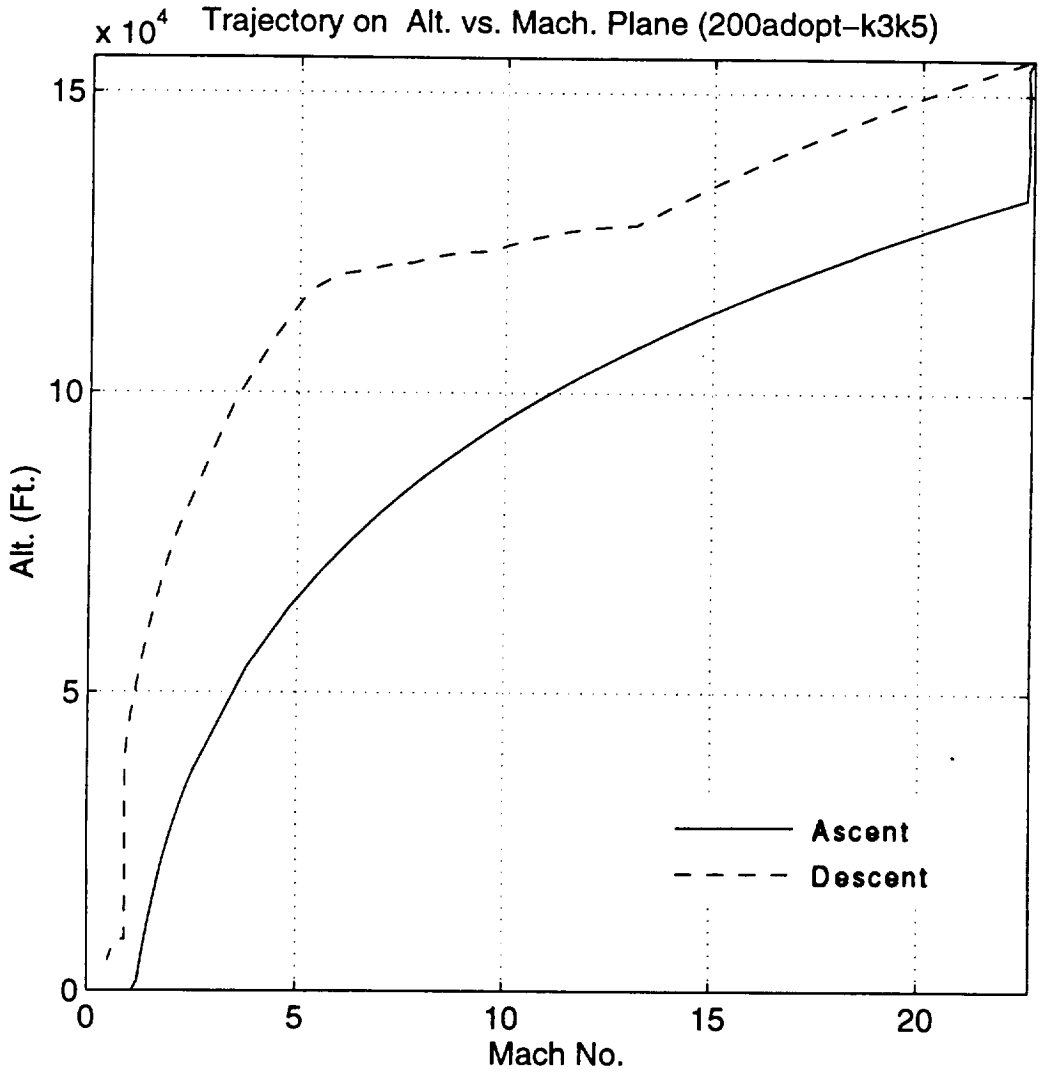

Figure 4. ABLV trajectory in min. time.

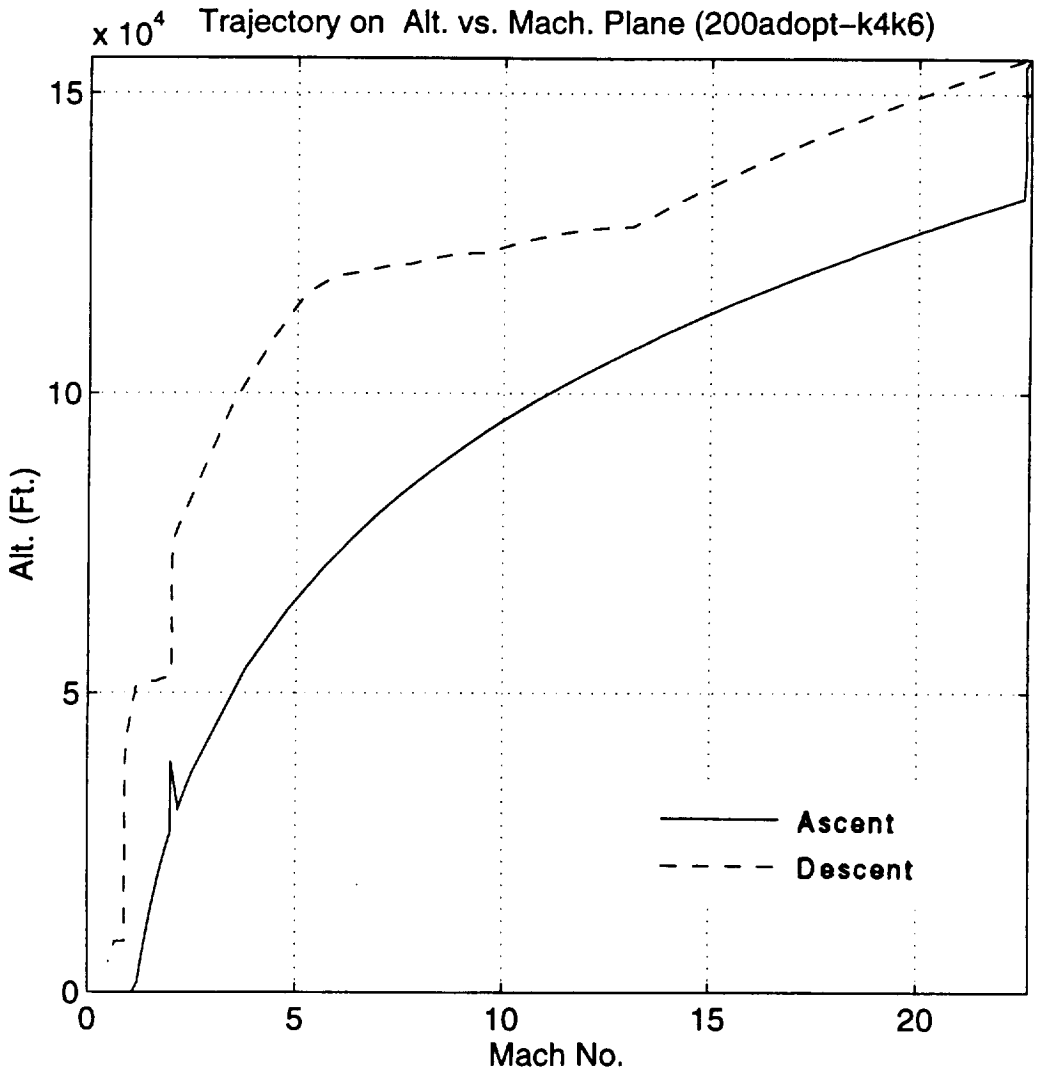

Figure 5. ABLV trajectory in min. heat-inlet.

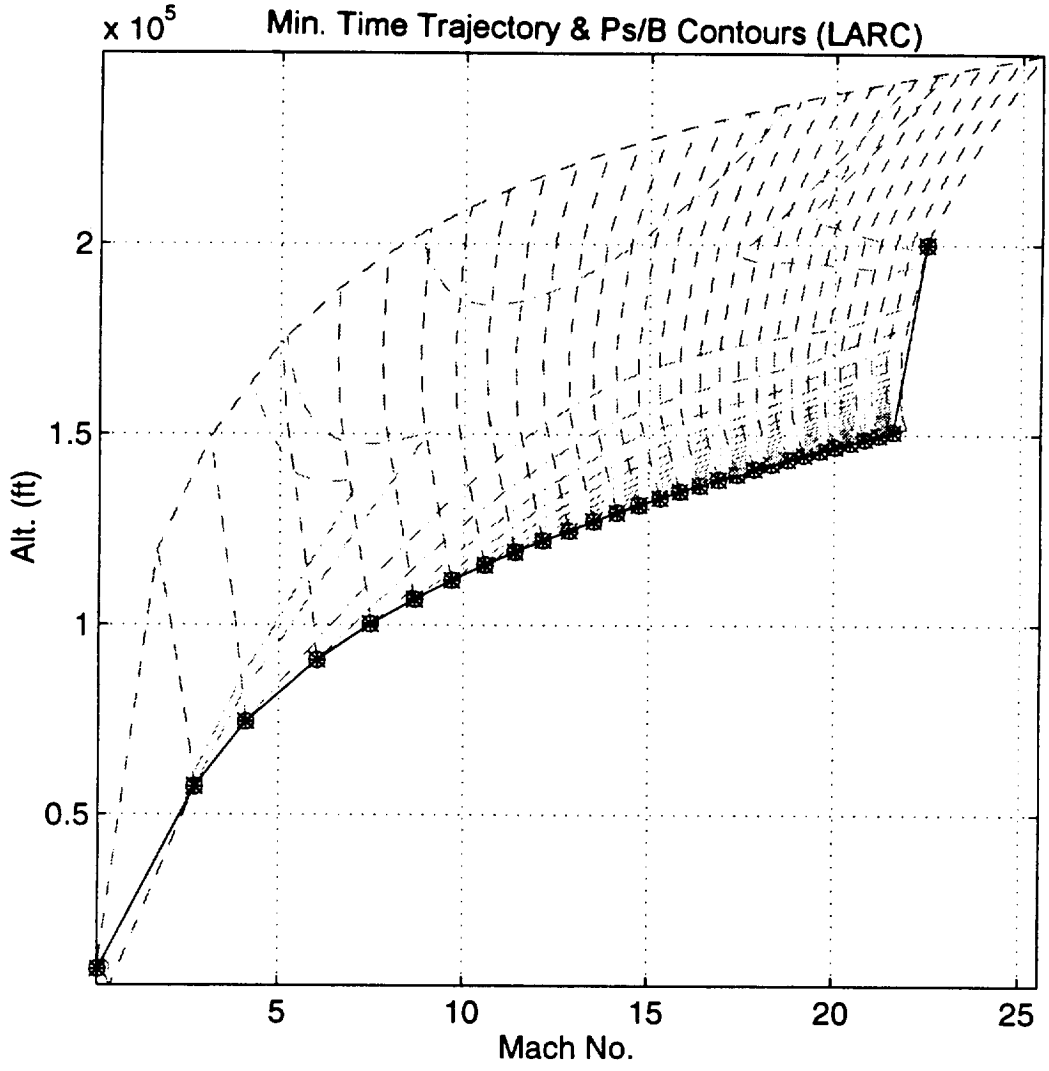

Figure 6. Reentry trajectory of SSTO all-rocket launch vechicle in min. time.

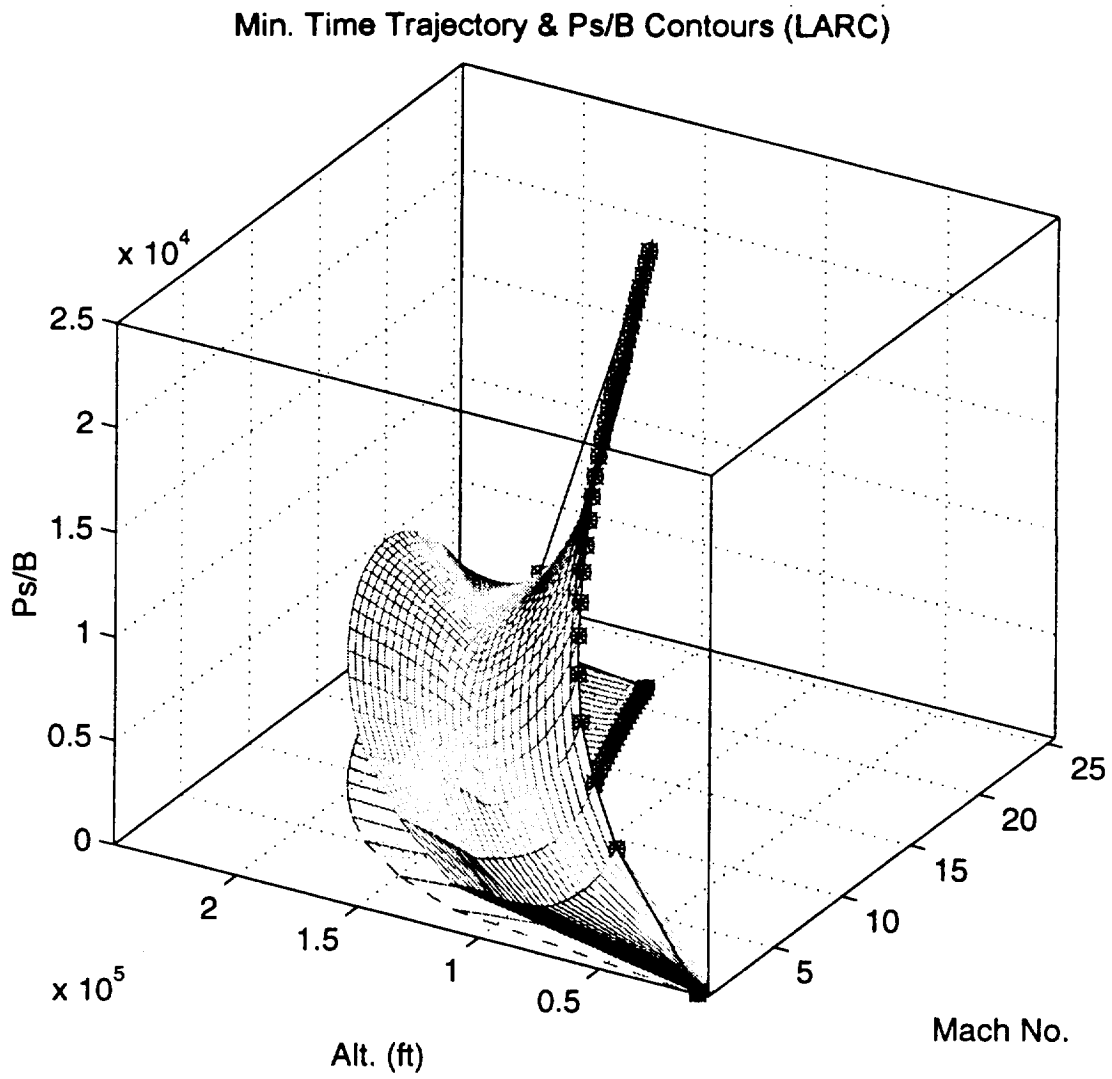

Figure 7. Cost functional mesh and reentry trajectory of SSTO all-rocket launch vechicle in min. time.

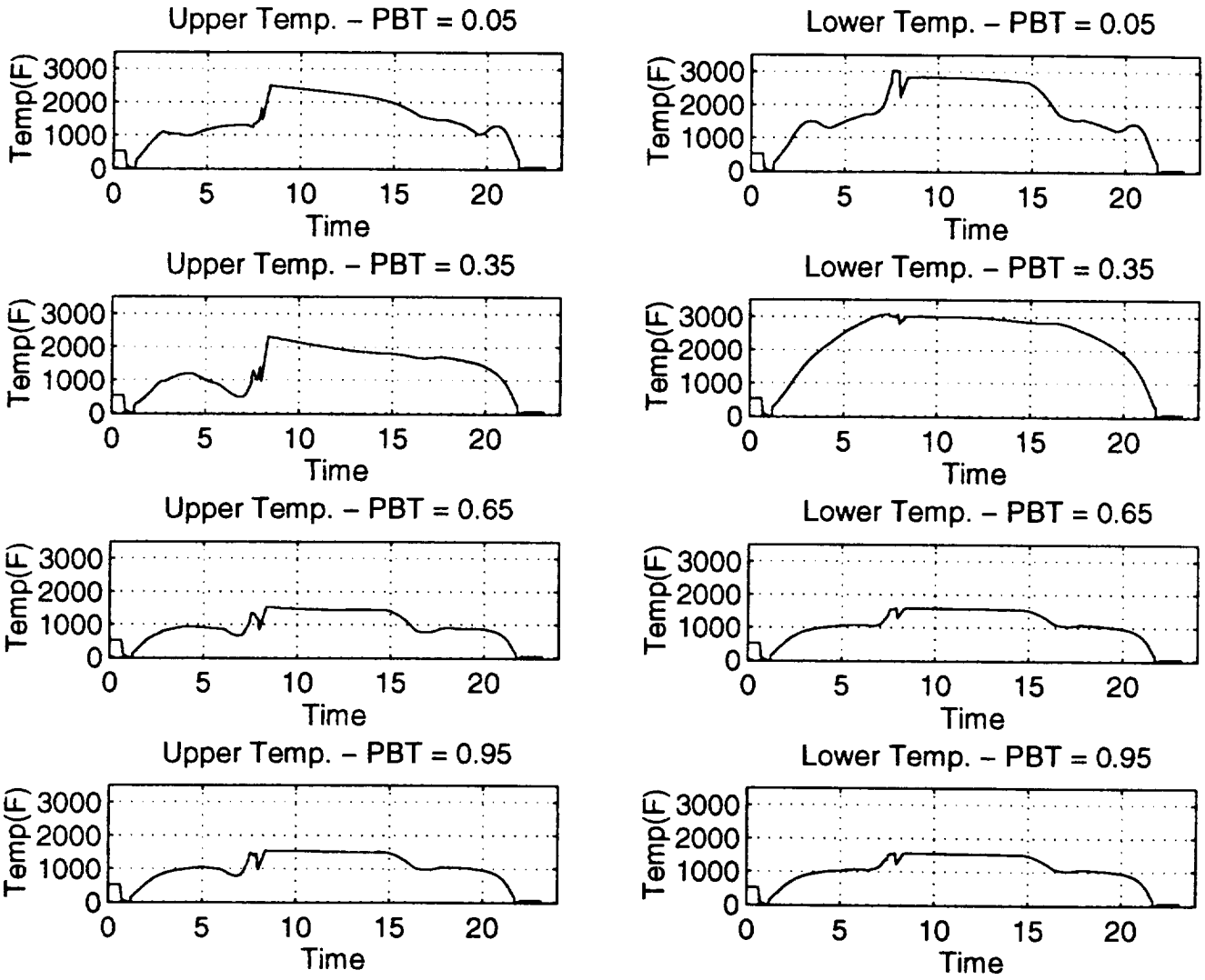

Figure 8. Time histories of temperature of SSTO all-rocket launch vechicle in min. time.

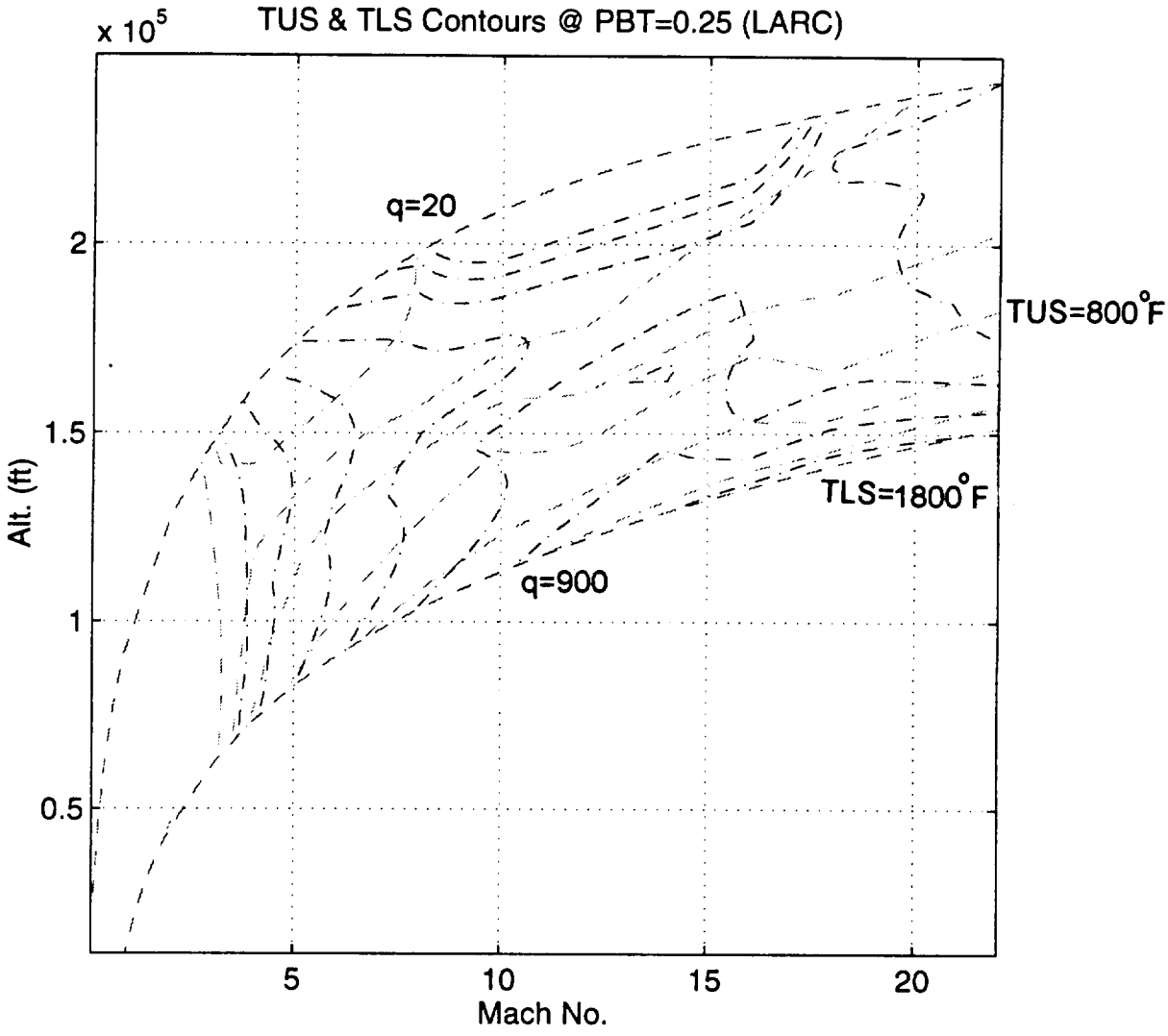

Figure 9. Teperature contours of TUS &TLS at PBT=0.25 of SSTO all-rocket launch vechicle.

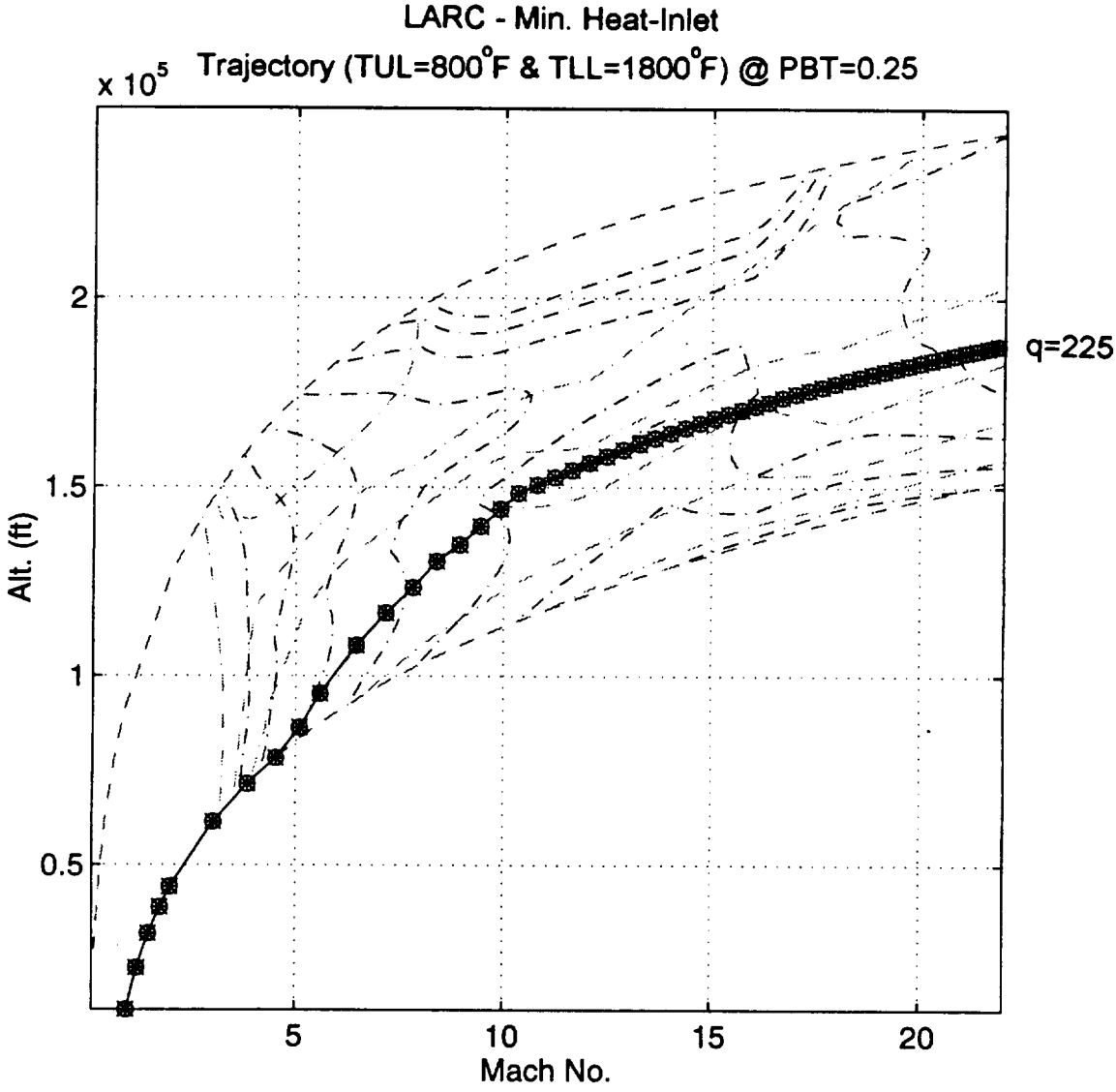

Figure 10. Reentry trajectory of SSTO all-rocket launch vechicle in min heat-inlet under temperature constraints.

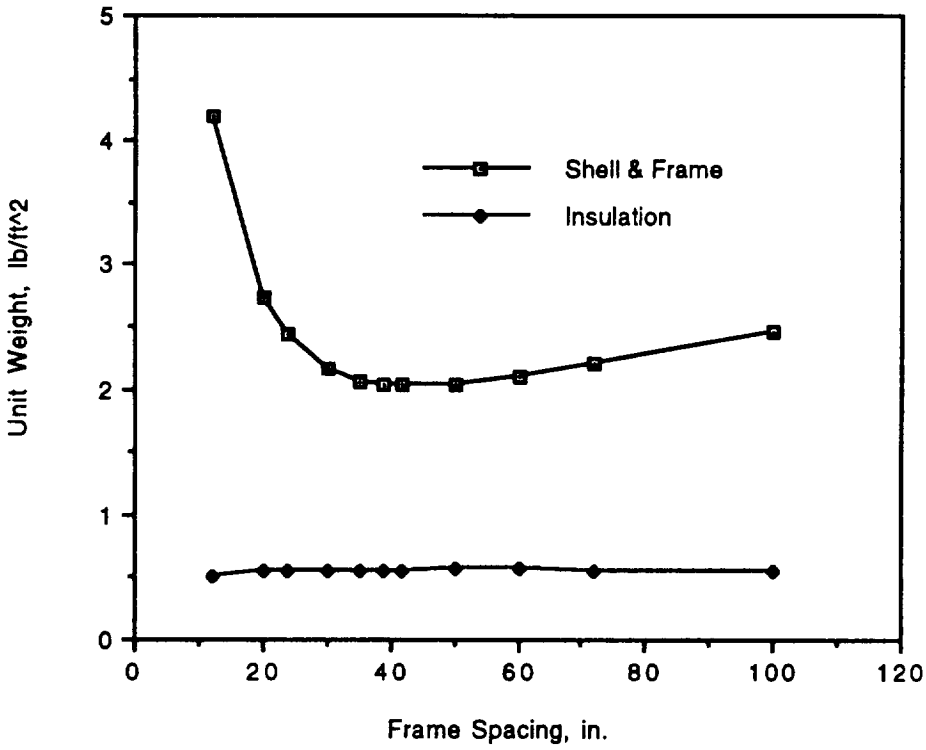

Figure 11. Unit weights vs. frame spacing, take-off weight = 2,500,000 lb.

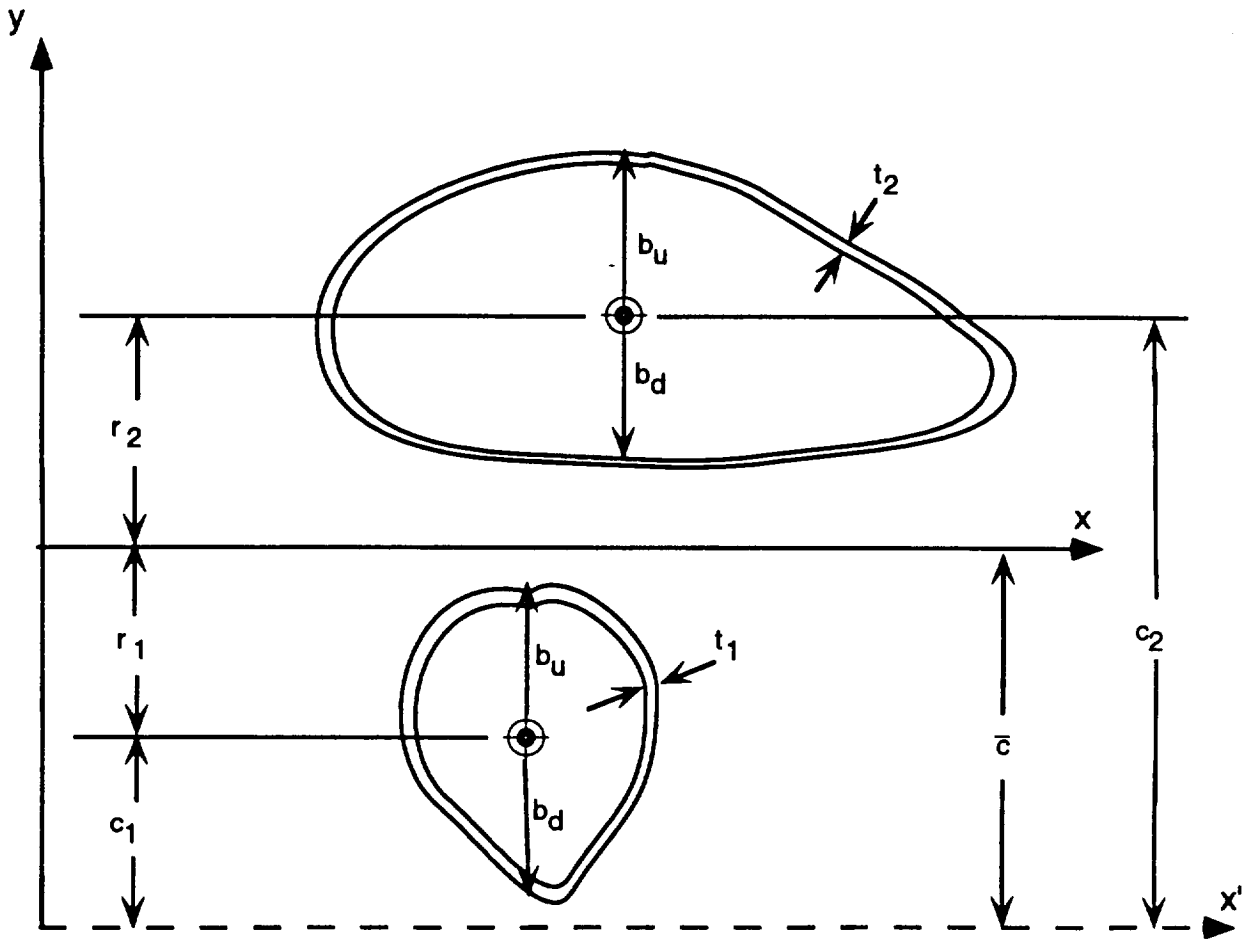

Figure 12. Thin-walled beams in bending.

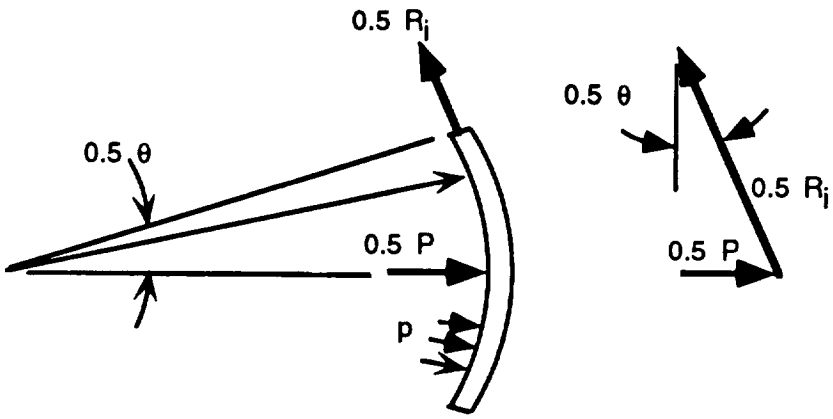

Figure 13. Single shell tank, internal pressure, hoop loading.

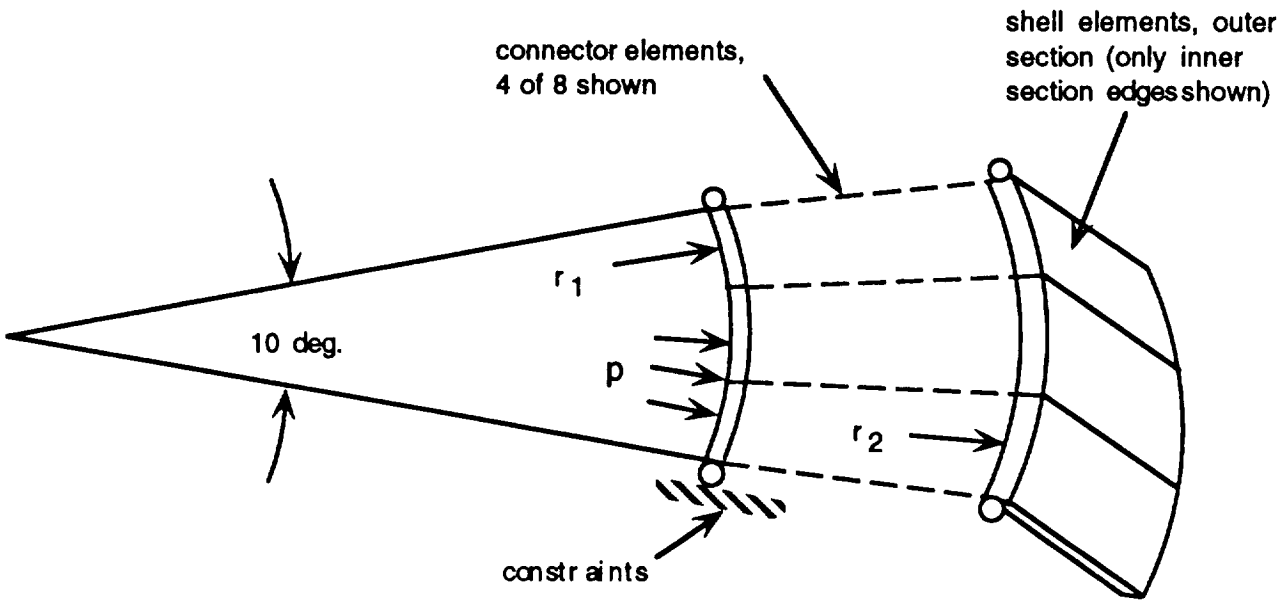

Figure 14. 2-shell finite element model, internal pressure.

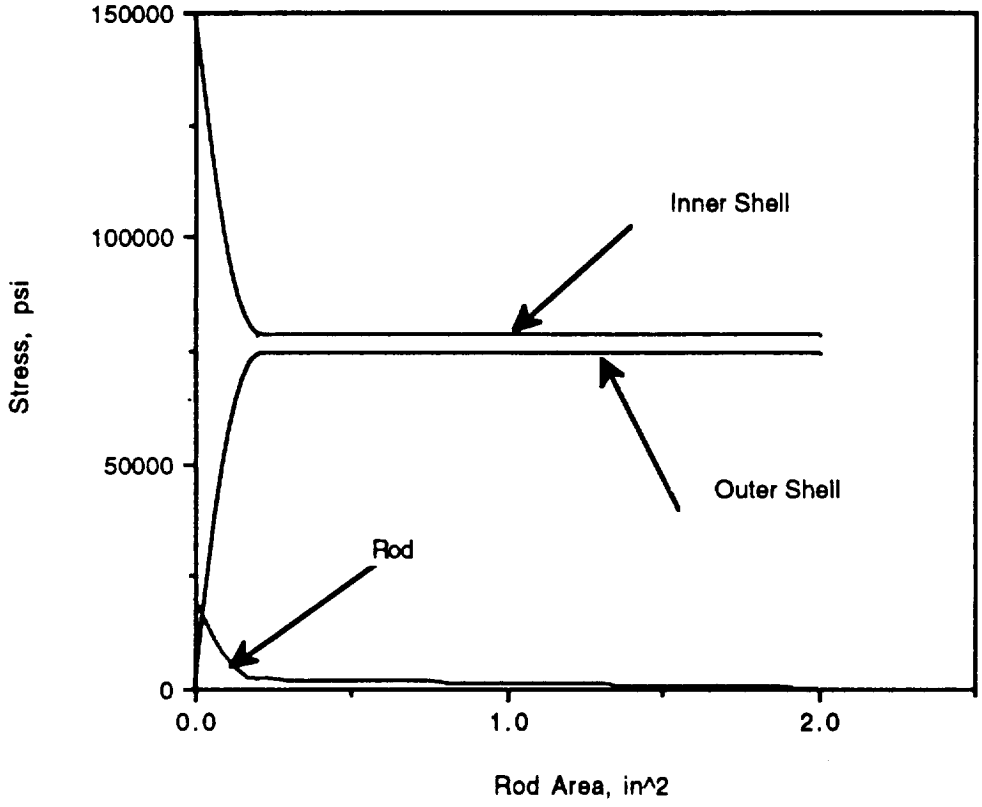

Figure 15. Shell stress, 12" by 10" rod spacing.

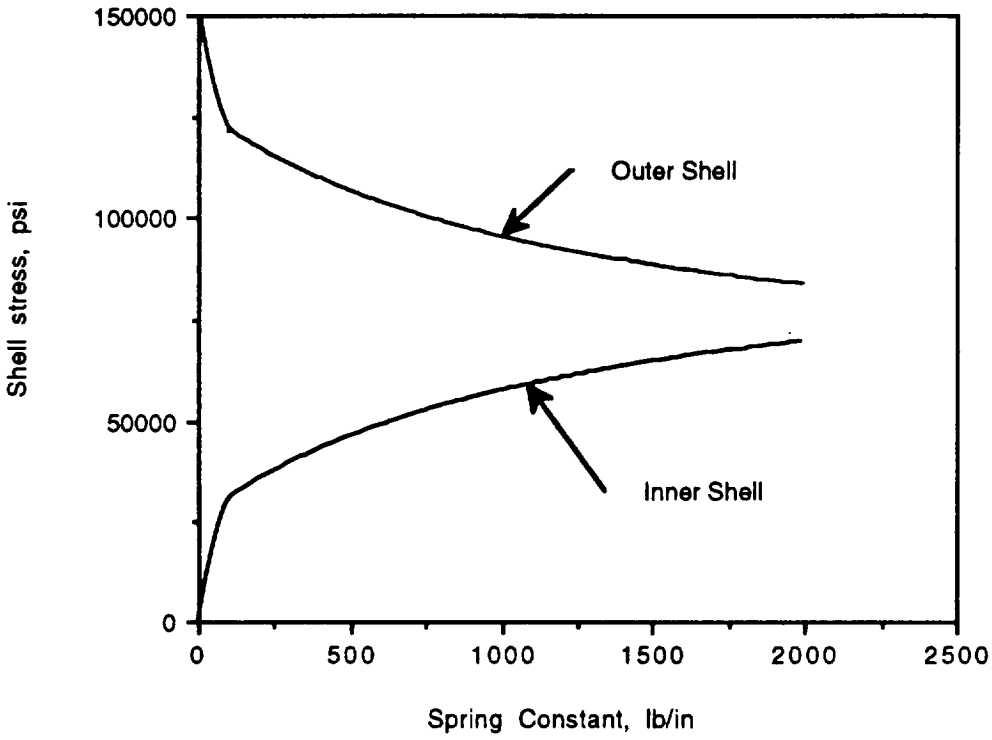

Figure 16. Shell stress, elastic suspension spaced 10" by 12".

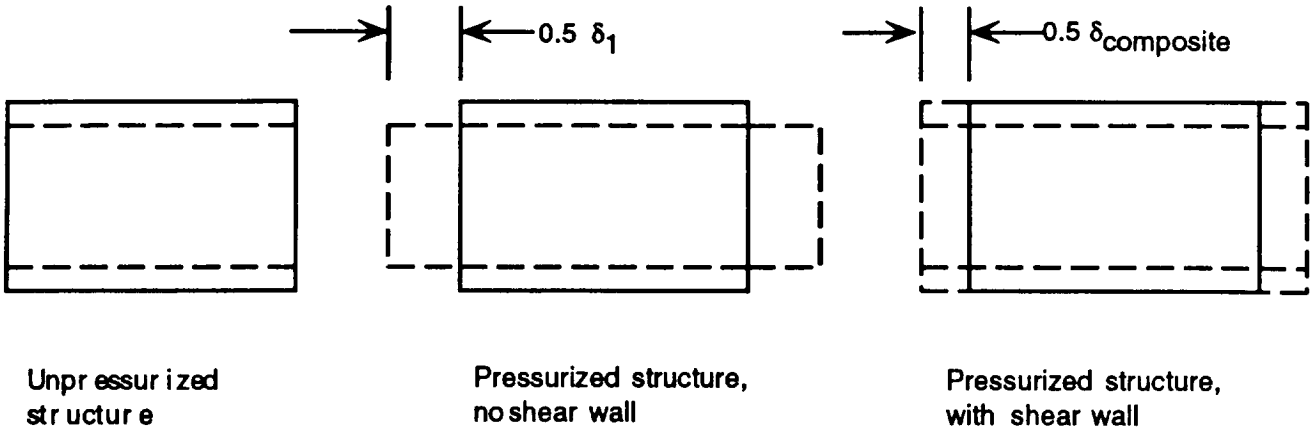

Figure 17. Axial deformation of concentric tanks, tank #1 under internal pressure.

Appendix A

AIAA-94-3635
Near-Optimal Propulsion System Operation for Air-Breathing Launch Vehicles
(Also accepted by *Journal of Spacecraft and Rockets*)

AIAA-94-3635

Near-Optimal Propulsion System Operation for Air-Breathing Launch Vehicles

M. Ardema
Santa Clara University
Santa Clara, California

J. Bowles
Nasa Ames Research Center

T. Whittaker
Sterling Software

AIAA Guidance, Navigation, and Control Conference
August 1-3, 1994 / Scottsdale, AZ

For permission to copy or republish, contact the American Institute of Aeronautics and Astronautics
370 L'Enfant Promenade, S.W., Washington, D.C. 20024

Near-Optimal Propulsion System Operation for Air-Breathing Launch Vehicles

M. D. Ardema*
Santa Clara University

J. V. Bowles**
NASA Ames Research Center

T. Whittaker***
Sterling Software

ORIGINAL PAGE IS OF POOR QUALITY

Abstract

A methodology for determining the near-optimal operation of the propulsion system of hybrid air-breathing launch vehicles is derived. The method is based on selecting propulsion system modes and parameters that maximize a certain performance function. This function is derived from consideration of the energy-state model of the aircraft equations of motion. The vehicle model reflects the many interactions and complexities of the multi-mode air-breathing and rocket engine systems proposed for launch vehicle use. The method is used to investigate the optimal throttle switching of air-breathing and rocket engine modes, and to investigate the desirability of using liquid oxygen augmentation in air-breathing engine cycles, the oxygen either carried from take-off or collected in flight.

Introduction

Studies are underway to select the next generation of space launch vehicles. The main incentive is to dramatically reduce the cost of access to space. The key to achieving this goal is thought to be use of vehicle systems that are completely reusable and operationally more like current aircraft than current launch vehicles.

One launch vehicle candidate is a single-stage-to orbit (SSTO) airplane that accelerates within the atmosphere with air-breathing engines for a substantial portion of its flight. This concept has been developed under the National Aerospace Plane program. Such an airplane is considerably different than any aircraft ever built and flown, and its development presents many challenges, most notably the design and operation of the propulsion system.

---

*Professor and Chairman, Dept. of Mechanical Engineering, Associate Fellow AIAA

**Aerospace Engineer

***Programmer/Analyst

PRECEDING PAGE BLANK NOT FILMED

This paper presents a method of determining the near optimal operation of the propulsion system of a SSTO hybrid air-breathing launch vehicle (ABLV). The method is suitable for use in a vehicle synthesis or preliminary design computer code, where ease of use and minimal calculation time are required. It would also be suitable as an on-board automatic propulsion system controller.

Several authors have developed simplified trajectory analyses for ABLV's, and most of these include propulsion system optimization schemes (Refs. 1-6). All of these analyses are based on reduced order modeling, and most employ the energy-state approximation. The approach in this paper is an extension and refinement of the method developed in Refs. 5 and 6.

Analysis of ABLV engine operation must account for the following features (most are unique to hypersonic vehicles):

(1) Because of the wide speed range of the vehicle, several different engine types are required; typically these are a low speed turbomachinery system, a ramjet, a scramjet, and a rocket. The performance of one engine type is often dependent on the performance of another type which may be in operation simultaneously.

(2) An engine type may have several modes of operation. For example, the flow of air into the scramjet may be augmented with liquid oxygen (LOX); this LOX may be carried in tanks at take-off or may be collected from the atmosphere at lower speeds. As another example, the rocket engine may be of dual fuel type; that is, able to burn two propellent fuels simultaneously in a controllable ratio.

(3) The scramjet engine requires a minimum fuel flow rate for cooling of the engine/airframe structure. The cooling flow requirement depends on speed, altitude, amount of LOX augmentation and several other variables, and can be as much as three times the flow required for stoichiometric combustion at higher Mach numbers.

(4) Vehicle angle-of-attack (α) has a strong affect on air-breathing engine thrust; because the forebody acts as an inlet ramp, the mass capture of the engine is nearly directly proportional to α.

(5) Many of the engine types have a net thrust vector that makes a significant angle with the vehicle longitudinal centerline, up to as much as 50°. This decreases thrust along the velocity vector, affects required aerodynamic lift, and impacts the performance of other engine types through α effects.

(6) Because of the low density of liquid hydrogen (LH2) fuel, hypersonic vehicles are sensitive to fuel volume as well as fuel mass. Consequently, both must be accounted for in any optimization criteria.

The analyses of Refs. 1-4 each account for some, but not all, of these features. Our approach incorporates all six. This is accomplished by a suitable choice of cost functional and by modeling the vehicle with the Hypersonic Air Vehicle Optimization Code (HAVOC), briefly described in Refs. 5 and 6. This code has been developed specifically to model the inter-disciplinary interactions in hypersonic aircraft and to provide accurate preliminary estimates of vehicle performance. It has

ORIGINAL PAGE IS
OF POOR QUALITY

been validated by extensive comparison with detailed hypersonic vehicle designs.

Derivation of Propulsion System Optimization Function

The derivation begins with the singularly perturbed equations of motion of a point-mass airplane with the following assumptions: (1) the aircraft flies in a great circle about a spherical, rotating Earth (terms in the square of the Earth's rotational speed are neglected), (2) the time rate of change of the flight path angle is neglected, (3) the effect of side-slip on vehicle drag is ignored (side-slip is necessary to maintain great-circle flight over a rotating Earth), and (4) zero ambient winds. Under these assumptions, the equations are

$$\begin{aligned} \epsilon\dot{h} &= V\sin\gamma \\ \dot{E} &= \frac{V}{mg_s}(T_v - D) = P \\ \dot{m} &= -\beta \\ 0 &= \frac{V\cos\gamma}{R+h} - \frac{g\cos\gamma}{V} + \frac{T_\gamma + L}{mV} + 2\Omega_\gamma \\ 0 &= T_s - 2m(\Omega_r V\cos\gamma - \Omega_T V\sin\gamma) \end{aligned} \tag{1}$$

In these equations, the state variables are h, the height above the surface of the Earth, E, the total mechanical energy, m, the vehicle mass, and γ the flight path angle; T_V, T_γ, and T_S are the components of thrust along the velocity vector, perpendicular to the velocity vector and in the great circle, and perpendicular to the great circle, respectively; D is drag; R is the radius of the Earth; g_s is the sea level gravitational acceleration; g is the local gravitational acceleration; and Ω_γ, Ω_r, and Ω_T are the Earth rotation (Coriolis) terms, which depend on instantaneous heading and latitude, as well as on speed and Earth rotation rate. The control variables are α, the angle of attack, and β, the engine fuel mass flow rate. Energy, altitude, and velocity are related by the equation.

$$E = \frac{hR}{R+h} + \frac{1}{2g_s}V^2 \tag{2}$$

Eqns. (1) with $\epsilon = 1$ are the trajectory equations used in the HAVOC code.

In Eqns. (1), the singular perturbation parameter ϵ has been inserted in such a way as to give the energy-state approximation when $\epsilon = 0$:

$$\begin{aligned} \dot{E} &= P \\ \dot{m} &= -\beta \end{aligned} \tag{3}$$

To be useful, these equations must be dependent only on altitude, h, and speed, V. In general, however, P also depends on angle of attack α, which couples the energy state equation to the other equations in Eq. 1. In subsonic aircraft, this dependency is generally eliminated by assuming that the thrust vector is aligned with the velocity vector and by evaluating the drag with lift equalized to weight. For hypersonic aircraft, however, the dependence of P on α is quite complicated and significant. First, the thrust vector is considerably offset from the velocity vector, and it is only the component along the velocity vector that affects p. Second, the air-breathing engine thrust magnitude also depends on α, because α affects the mass capture area and thus the airflow into the engine. Finally, if both a rocket engine and an air-breathing engine are operating simultaneously, the rocket throttle setting affects air-breather thrust through α effects. All of these

effects are accounted for in the present paper, and, consistent with energy-state approximation, the value of α used to evaluate P is determined by enforcing equilibrium in the airplane plane of symmetry perpendicular to the velocity vector.

For a SSTO mission with a hypersonic aircraft, what is desired is a trajectory that gives the minimum gross take-off weight vehicle to put a given payload mass and volume in orbit. Because liquid hydrogen fueled aircraft have relatively low gross densities and correspondingly high surface area to gross weight ratios, they are sensitive to perturbations in volume as well as in mass; and it is therefore necessary to minimize a weighted sum of fuel mass and volume. Thus, the quantity to be minimized is:

$$\phi = -(m_f + KV_f) \tag{4}$$

where m_f and V_f are the fuel mass and volume, respectively, and $K \in [0, \infty)$ is a weighting parameter, to be determined shortly.

Another feature of ABLV's that needs to be taken into account is that they have typically several independent (more or less) propulsion modes. If there are n modes, the total thrust (along the velocity vector) and fuel flow rates are

$$\begin{aligned} T_V &= f_V \sum_{i=1}^{n} \pi_i T_{M_i} \cos(\alpha + \delta_i) \\ \beta &= \sum_{i=1}^{n} \beta_i = \sum_{i=1}^{n} C_i \pi_i T_{M_i} \end{aligned} \tag{5}$$

where, for each mode, $\pi_i \in [0,1]$ is throttle setting, T_{M_i} is maximum thrust, δ_i is thrust offset angle, C_i is thrust specific fuel consumption, and f_V is a parameter to account for the fact that the thrust vector has a component perpendicular to the aircraft plane of symmetry.

The quantity to be minimized for a given energy gain is

$$J' = \int_{\phi_0}^{\phi_f} d\phi = \int_{t_0}^{t_f} \dot{\phi} dt = \int_{E_0}^{E_f} \frac{\dot{\phi}}{P} dE \tag{6}$$

where Eqn. (3) was used. It is assumed that $\dot{\phi} > 0$, $P > 0$ and that E is monotonically increasing. If the propellent density is $\rho = m_f / V_f$, then from Eqns. (3) and (4):

$$\dot{\phi} = -\left(\dot{m}_f + K \frac{\dot{m}_f}{\rho} \right) = \sum_{i=1}^{n} \beta_i \left(1 + \frac{K}{\rho_i} \right) \tag{7}$$

For convenience, we choose to invert the integrand in Eqn. (6) and maximize; from Eqns. (1), (5), (6), and (7), the quantity to be maximized is

$$J = \int_{E_0}^{E_f} F dE \tag{8}$$

where

$$F = \frac{V \left[f_v \sum_{i=1}^{n} \pi_i T_{M_i} \cos(\alpha + \delta_i) - D \right]}{m g_s \sum_{i=1}^{n} C_i \pi_i T_{M_i} \left(1 + \frac{K}{\rho_i} \right)} \tag{9}$$

If propulsion mode i has two propellants, with densities ρ_{1i} and ρ_{2i} (one of which may be LOX), and the ratio of flow rates is $\eta_i = \dot{m}_{1i} / \dot{m}_{2i}$, then the density to be used in Eqn. (9) is

$$\rho_i = \frac{\rho_{1_i}\rho_{2_i}(1+\eta_i)}{(\rho_{1_i}+\eta_i\rho_{2_i})} \qquad (10)$$

The vehicle angle of attack used in evaluating Eqn. (9) is determined by enforcing vertical equilibrium [see Eqn. (1)]:

$$0 = \frac{V}{R+h} - \frac{g}{V} + \frac{T_\gamma + L}{mV}\cos\phi + 2\Omega_\gamma \qquad (11)$$

Eqns. (8) and (9) may be used in many ways to study near-optimal ABLV design and operation. For example, if h (and a corresponding V) is chosen at each energy level to maximize F, then a near-optimal flight path, called the energy-climb path, is developed (see Refs. 5 and 6, for example). As another example, if two independent propulsion systems are available at one point in the flight envelope, evaluation of F will indicate which one, or both, should be operated. As a more complicated example, if an air-breathing mode uses LOX augmentation at one point in the climb path, the performance at other parts of the trajectory are affected because of the additional weight and volume the LOX and its tankage; this type of analysis requires the evaluation of the functional J.

In this paper, the flight path will be fixed, as shown in Fig. 1, and attention will be focused on the operation of the propulsion system. Two representative problems will be studied to illustrate the approach. First, the near-optimal throttle switching between air-breathing and rocket engines will be determined, and second, near-optimal use of LOX augmentation in the scram jet engine will be addressed. The flight path is for a launch due east at latitude 35°, and then acceleration to Mach 25.265 following dynamic pressure and heating constraints.

Before proceeding with these analyses, the optimal value of K will be determined. This is done numerically by computing "closed vehicles" for a range of values of K; that is, iteratively exercising the HAVOC code to obtain the gross take-off weight and volume required to put a specified payload weight and volume in a specified orbit. The result for a typical ABLV is shown in Fig. 2. It is seen that a value of $K = 3$, with fuel density in lbs/ft^3, denoted hereafter by K^*, gives very nearly a minimum of both take-off weight and empty weight, and this value will be used throughout the rest of the paper. The figure shows that use of the optimally weighted cost functional saves 4% in gross weight and 5% in empty weight, relative to minimizing fuel weight only.

Optimal Airbreather/ Rocket Throttle Switching

Now assume that there are two independent propulsion modes, an airbreathing engine mode and a rocket engine. It is desired to develop an algorithm for optimal throttle selection for the two modes. This problem has been addressed in Refs. 1, 2, 3, 5, and 6. In this section, the approach of Refs. 5 and 6 is reviewed and extended.

The function F is now

$$= \frac{V\left(f_V\pi_a T_{M_a}\cos(\alpha+\delta_a) + f_V\pi_r T_{M_r}\cos(\alpha+\delta_r)\right) - l}{mg_s\left(C_a\pi_a T_{M_a}\left(1+\frac{K}{\rho_a}\right) + C_r\pi_r T_{M_r}\left(1+\frac{K}{\rho_r}\right)\right)} \qquad (12)$$

where subscripts a and r denote airbreather and rocket, respectively. The controls are now the throttle settings, $\pi_a \in [0,1]$ and $\pi_r \in [0,1]$. If ρ_H and ρ_O are the densities of LH2 and LOX, respectively, then $\rho_a = \rho_H$ and, from Eqn. (10)

$$\rho_r = \frac{\rho_O \rho_H (1+\eta_r)}{(\rho_O + \eta_r \rho_H)} \tag{13}$$

where η_r is the oxidizer-to-fuel flow ratio of the rocket.

The constraints on the airbreather fuel flow rate are very complicated, and best discussed in terms of e, the equivalence ratio, defined as the ratio of actual fuel flow to the fuel flow for stoichiometric combustion. At about Mach 6, the end of the ramjet mode and the start of the scram jet mode of the airbreathing engine, there may be a pronounced reduction in the allowable e due to thermal choke and burner exit Mach number limits for the variable geometry scramjet engines, resulting in full available throttle, $\pi_a = 1$, corresponding to $e < 1$ in this region of the flight path. Another important constraint is the need to circulate the LH2 fuel through the engine structure before combustion in order to cool the engine structure. This requires a higher fuel flow rate than stoichiometric at high Mach numbers, and thus $\pi_a = 1$ corresponds to $e > 1$ in this region. When $e = 1$ is allowed, $\pi_a = 1$ corresponds to $e = 1$. The constraints on e are discussed in detail in Refs. 5 and 6. The constraints on rocket throttle, π_r, are simple bounds independent of Mach number.

The maximization of F as given by Eqn. (12) is now straightforward. Let

$$\psi = \frac{C_a\left(1+\frac{K}{\rho_a}\right)\cos(\alpha+\delta_r)}{C_r\left(1+\frac{K}{\rho_r}\right)\cos(\alpha+\delta_a)} \tag{14}$$

Then the optimal throttle selection control law is as follows:

If $\psi \geq 1$, then

$$\pi_r = 1$$
$$\pi_a = \begin{cases} 0, \text{ if } 1 - \dfrac{D}{f_v T_{M_r} \cos(\alpha+\delta_r)} > \dfrac{1}{\psi} \\ 1, \text{ otherwise} \end{cases} \tag{15}$$

If $\psi < 1$, then

$$\pi_a = 1$$
$$\pi_r = \begin{cases} 0, \text{ if } 1 - \dfrac{D}{f_v T_{M_a} \cos(\alpha+\delta_a)} > \psi \\ 1, \text{ otherwise} \end{cases}$$

This control law may be interpreted as follows. First, the mode that is most fuel efficient in generating thrust along the velocity vector is turned on (the test on ψ); call this mode one. Then, mode two is turned on, additionally, if a second test is satisfied. This second test depends on both the thrust-to-drag ratio of mode one operation, as well as the relative efficiencies of the two modes. Note that if the thrust of mode one is less than the drag, mode two is always turned on. Note also that both modes are always either on full or completely off.

Fig. 3 shows the test function ψ as a function of Mach for three values of K. As expected, the higher the value of K, the higher the premium on minimizing fuel volume, and thus on using the rocket more and the airbreather less. The associated throttle histories are shown on Fig. 4. For $K = 3$ and $K = 0$, the airbreather is on continuously to the end of the trajectory. The rocket comes on at a high hypersonic Mach, higher for the K=0 case than for K=3. For K=20, the airbreather is turned off before the end of the trajectory, and the rocket comes on much earlier. In all cases, the rocket is used for take-off acceleration augmentation; in fact, this is what sizes the rocket.

Scramjet Engine Liquid Oxygen Augmentation

Hypersonic air-breathing propulsion systems produce thrust by processing free stream air; compressing the air, typically through a series of external and internal ramps, combusting the high pressure air with fuel to add heat, and expanding the combustion product gases through a nozzle. The more air that is processed, say by flying at higher dynamic pressures, the higher the engine thrust. At high Mach numbers, air-breathing hypersonic vehicles encounter increased aerothermal heating, which at first requires the engine fuel flow to be higher than the stoichiometric value due to airframe and engine cooling needs, and eventually forcing the vehicle to fly a lower dynamic pressure trajectory dictated by material temperature limits. The resulting higher altitude/lower dynamic pressure flight path results in a decrease in air-breather thrust, which can be compensated for by several means, including use of a rocket engine.

Another alternative propulsion enhancement method is the use of oxidizer-augmentation and preburning in the hypersonic scramjet engine. In an oxidizer-augmented combustor, fuel is pre-mixed with on-board stored oxidizer in a secondary combustion chamber, and the combustion products are injected into the main airflow path, resulting in improved combustor performance at high Mach numbers, enhanced combustor stream force, and overall higher propulsion system thrust. The higher engine thrust levels are achieved at the expense of higher engine thrust-specific fuel consumption, due to higher on-board mass flow. Thrust off-set angles and engine cooling requirements are changed as well. Burning the fuel with on-board oxidizer, which could be liquid oxygen (LOX) or liquid air, is usually done fuel-rich to assure efficient combustion in the preburner, and enhanced mixing of the unburned fuel with the airflow stream in the main combustion chamber. The LOX augmented engine has higher specific thrust compared to the liquid air concept due to higher combustion temperatures. The oxidizer must be in liquid state to allow combustion in the "imbedded rocket" engine, i.e. the preburner.

The LOX could be stored on-board the vehicle at takeoff, or air collected and liquefied by cryogenic fuel during the assent. The scramjet augmentation could then use either liquid air preburning, or the oxygen could be separated during the liquefaction process.

For the present study, the HAVOC code has been modified to model all these complex interactions involved in LOX augmented scramjet engine performance.

In this section, we will investigate whether or not this LOX augmentation is beneficial, and, if it is, determine: (i) where in the flight path it should be used, (ii) how much should be used, and (iii) whether it should be carried from the ground or collected en route.

The approach to optimizing the use of LOX augmentation is similar to determining optimal throttle switching; the function F in Eqn. (12) is maximized with respect to the amount of augmentation at each point along the flight path. A typical result is shown in Fig. 5. This figure plots η_a, the ratio of LOX-to-LH2 mass flow to the scram jet engine, as a function of M. It is seen that LOX augmentation begins at about Mach 18, reaches the maximum allowable level at a slightly higher M, and stays at that level until the end of the flight path. Figure 6 shows that the fuel rate goes up dramatically when augmentation is used; on the other hand, the longitudinal acceleration also greatly increases (Figure 7) giving shorter flight times. The net result is that with LOX augmentation a higher final vehicle weight is obtained, as shown on Figure 8.

It was found that the optimal use of augmentation is highly dependent on modeled scramjet performance. For example, if the non-augmented specific fuel consumption is reduced by 10%, or if the augmented fuel consumption is increased by 10%, augmentation is not optimal.

Now consider the issue of whether it is best to store the LOX to be used for augmentation on board at take-off, or if it is best to collect air during the flight. The latter has the advantage that the take-off weight will be lower, and thus the performance at low speeds will be better, but the disadvantage that the drag will be higher during air collection. Obviously, air collection will be better when the advantage is greater than the disadvantage. Because two different segments of the trajectory are involved, this issue cannot be decided by point-wise evaluation of the function F; rather, the integrated performance J must be evaluated.

Suppose that the trajectory begins at energy level E_0 and that subsequently air is collected between a small interval E_1 to E_2. The improvement in performance at E_1 due to a change in mass Δm from E_0 to E_1, to first order, is obtained from Eqn. (8) as

$$\Delta J_{01} = \left(\frac{dJ}{dm}\Delta m\right)_{01} = \Delta m \int_{E_0}^{E_1} \frac{dF}{dm} dE \quad (16)$$

If it is assumed that wing-loading is held constant as the airplane changes size and weight, both thrust and drag will tend to change linearly with changes in mass. Thus, from Eqn. (9), the only net dependence of F on m is via the explicit factor m and consequently $dF/dm = -F/m$. substitution into Eqn. (16) gives:

$$\Delta J_{01} = -\Delta m \int_{E_0}^{E_1} \frac{F}{m} dE \quad (17)$$

Next consider the change in performance due to collecting a mass of air Δm_{air} from E_1 to E_2. Again from Eqn. (8), to first order,

$$= \left(\frac{dJ}{dm}\Delta m_{air}\right)_{12} = \Delta m_{air}\int_{E_1}^{E_2}\frac{dF}{dm}dE = \Delta m_{air}\frac{dF}{dm} \quad (18)$$

where $\Delta E = E_2 - E_1$ is a small energy increment. Assuming that the only dependence on F of the air collection is through the drag term,

$$\frac{dF}{dm} = \frac{dF}{dD}\frac{dD}{dm} \quad (19)$$

From Eqn. (9),

$$\frac{dF}{dD} = -\frac{F}{(T_v - D)} \quad (20)$$

The drag associated with the air collection is

$$D = P_a A + \rho A V^2 \quad (21)$$

where P_a and ρ are the atmospheric static pressure and density, respectively, and A is the collection capture area. Thus

$$\frac{dD}{dm} = P_a\frac{dA}{dm} + \rho\frac{dA}{dm}V^2 \quad (22)$$

The mass captured during time Δt between E_1 and E_2 is $m = \rho A V \Delta t$ so that

$$\frac{dm}{dA} = \rho V \Delta t \quad (23)$$

Combining Eqns. (18), (19), (20), (22), and (23) gives

$$\Delta J_{12} = -\Delta m_{air}\frac{F}{(T_v - D)}\frac{(P_a + \rho V^2)}{\rho V}\frac{\Delta E}{\Delta t} \quad (24)$$

From Eqns. (1), $\Delta E/\Delta t = P$ so that Eqn. (24) becomes

$$\Delta J_{12} = -\Delta m\frac{F(P_a + \rho V^2)}{\rho m g_s \eta} \quad (25)$$

where all quantities are to be evaluated at E_1, and where η is the ratio of LOX mass to air mass ($\eta = .2315$).

Now let

$$Q_1 = \int_{E_0}^{E_1}\frac{F}{m}dE \quad (26)$$

$$Q_2 = \frac{F_1(P_{a_1} + \rho_1 V_1^2)}{\rho_1 m_1 g_s \eta} \quad (27)$$

Then, from Eqns. (17) and (25), air collection will be optimal compared with LOX storage when

$$Q_1 > Q_2 \quad (28)$$

Figure 9 shows the variation of Q_1 and Q_2 along the trajectory. It is seen that Inequality (28) is never satisfied. in fact, (28) would not be satisfied even if the atmosphere were 100% oxygen and thus air collection is clearly inferior to LOX storage from take-off. Also, weight penalties for air liquefaction and disposal of the nitrogen have not been included; including these penalties would increase the advantage of LOX storage.

Concluding Remarks

A cost functional based on energy-state approximation has been used to optimize propulsion system operation of a single-stage-to-orbit hybrid air-breathing launch vehicle. The first issue addressed was optimal throttle switching of rocket and airbreathing engine modes. It was found that in most cases the airbreathing mode was at full throttle for the entire ascent

trajectory, and the rocket was off until a high hypersonic speed, and then on full for the rest of the trajectory.

The use of liquid oxygen (LOX) augmentation in the scramjet engine was also considered. It was found that LOX augmentation is optimal at high hypersonic speeds, but this conclusion is sensitive to scramjet engine modeling. It was also determined that it is far better to carry the LOX from take-off rather than collecting and separating air during flight.

References

1. McDevitt, M.; Hames, J.; Bedford, R. "Trajectory and Propulsion Schedule Optimization Techniques for NASP." Lockheed Fort Worth Company unpublished report, 1990.

2. Corban, J.; Calise, A.; Flandro, G. "Rapid Near-Optimal Aerospace Plane Trajectory Generation and Guidance." J. Guidance, Control, Dynamics, vol. 14, no. 6, Nov.-Dec 1991, Pp. 1181.

3. Van Buren, M. and Mease, K. "Aerospace Plane Guidance Using Time-Scale Decomposition and Feedback Linearization." J. Guidance, Control, Dynamics, vol. 15, no. 5, Sept. Oct. 1992, Pp. 1166.

4. Lu, P. "Analytical Solutions to Constrained Hypersonic Flight Trajectories." J. Guidance, Control, Dynamics, vol. 16, no. 5, Sept.-Oct. 1993, Pp. 956.

5. Ardema, M.; Bowles, J.; Whittaker, T. "Optimal Trajectories for Hypersonic Launch Vehicles." Lecture Notes in Control and Information Sciences, vol. 170, Skowronski, et al., ed., Springer Verlag, 1992.

6. Ardema, M.; Bowles, J.; Terjesen, E.; Whittaker, T. "Near-Optimal Energy Transitions for Energy-State Trajectories of Hypersonic Aircraft." AIAA Paper 92-4300, presented at the AIAA Guidance, Navigation, and Control Conference, Hilton Head, SC, August 1992.

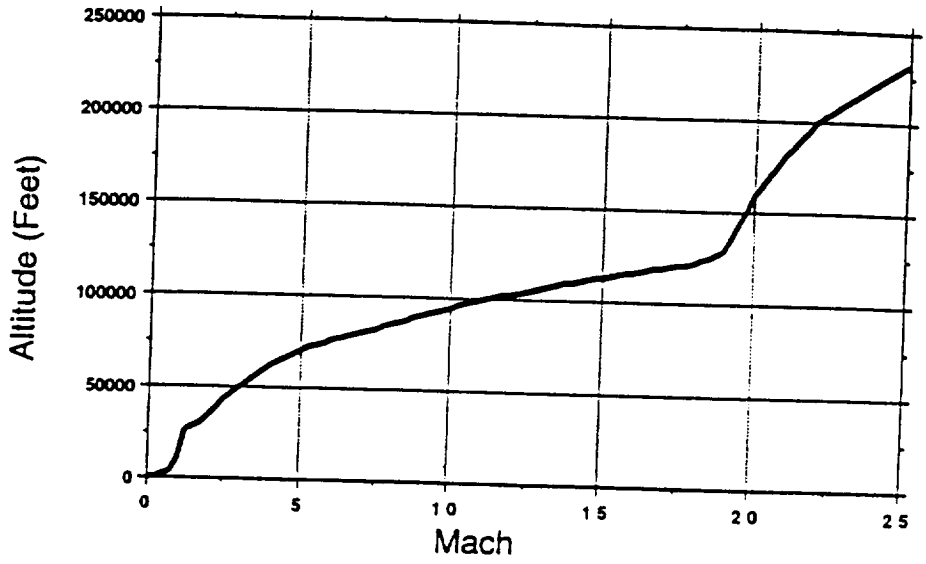

Figure 1. ABLV Trajectory

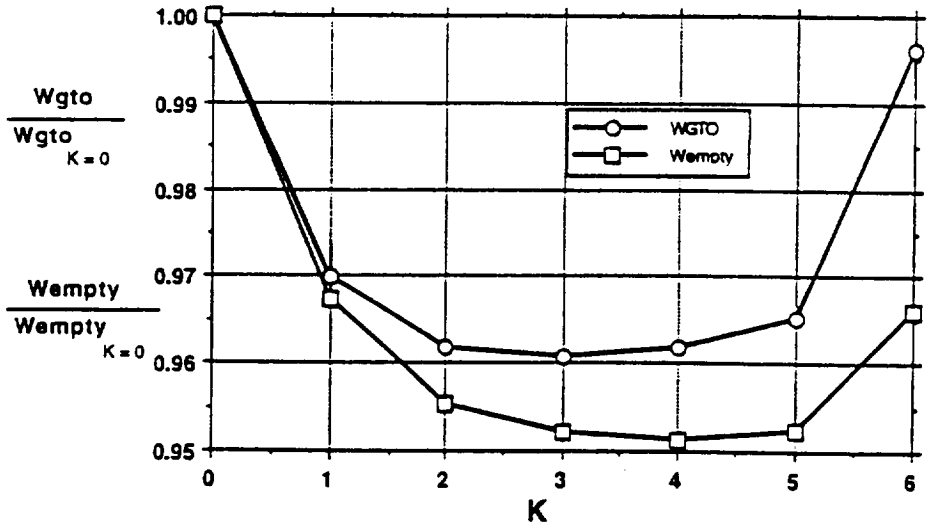

Figure 2. Effect of Weighting Parameter K

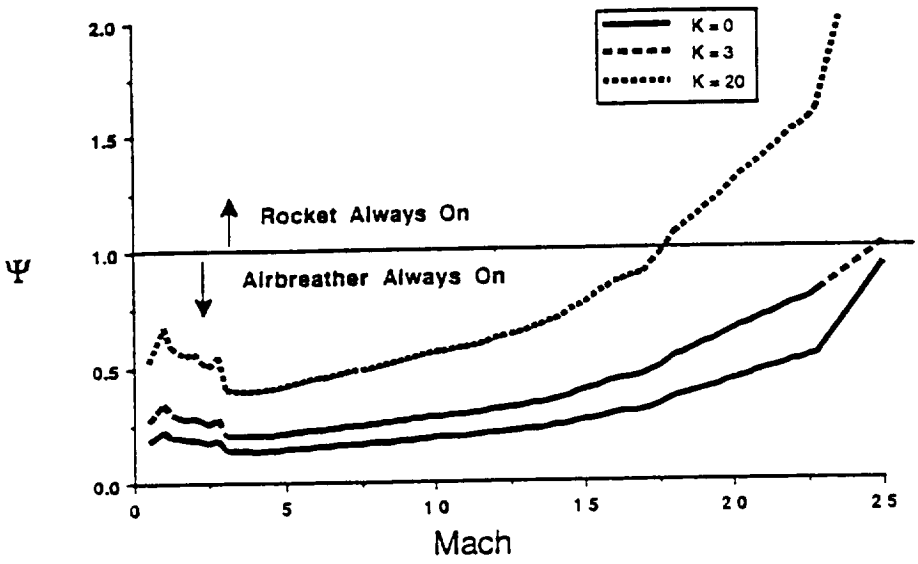

Figure 3. Throttle Switching Test Function

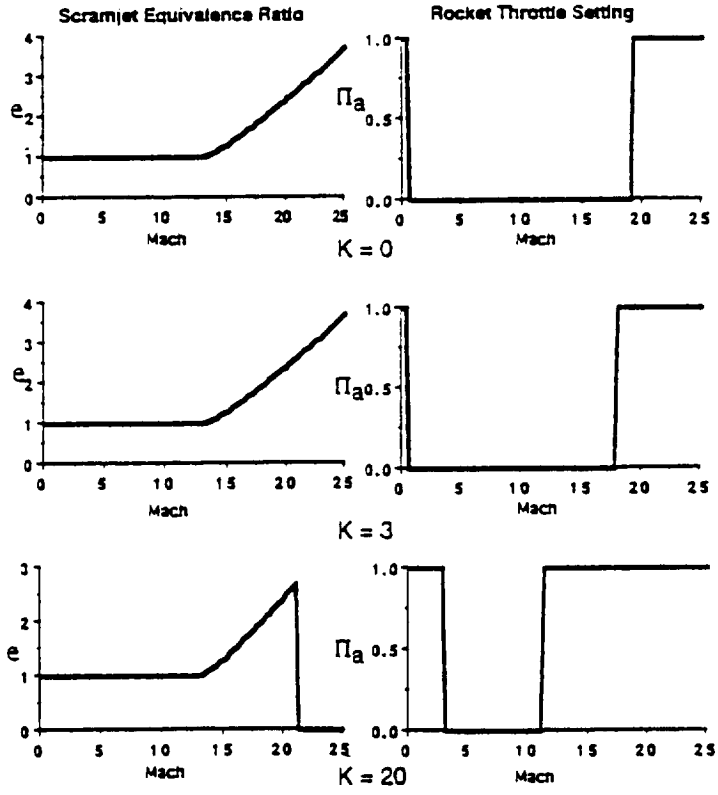

Figure 4. Optimal Throttle Schedules

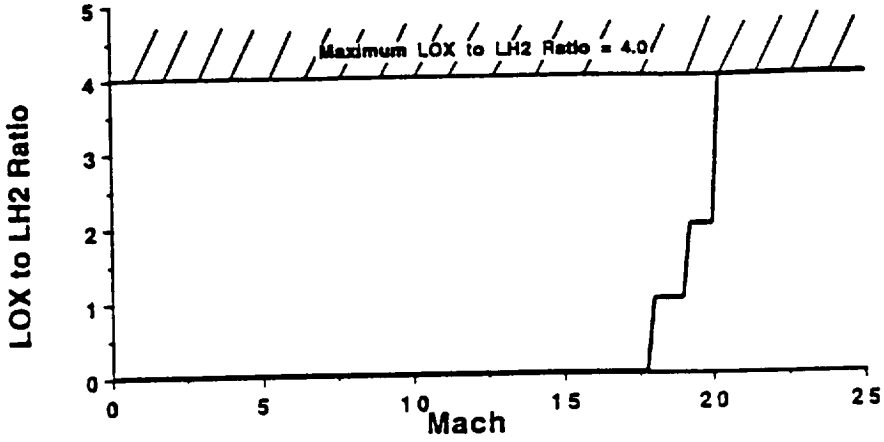

Figure 5. Optimal LOX Augmentation

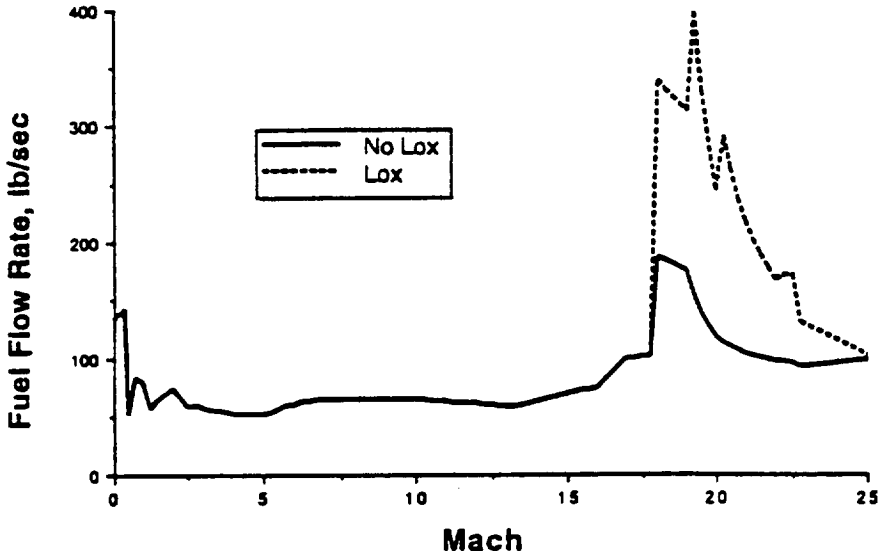

Figure 6. Fuel Flow Rates

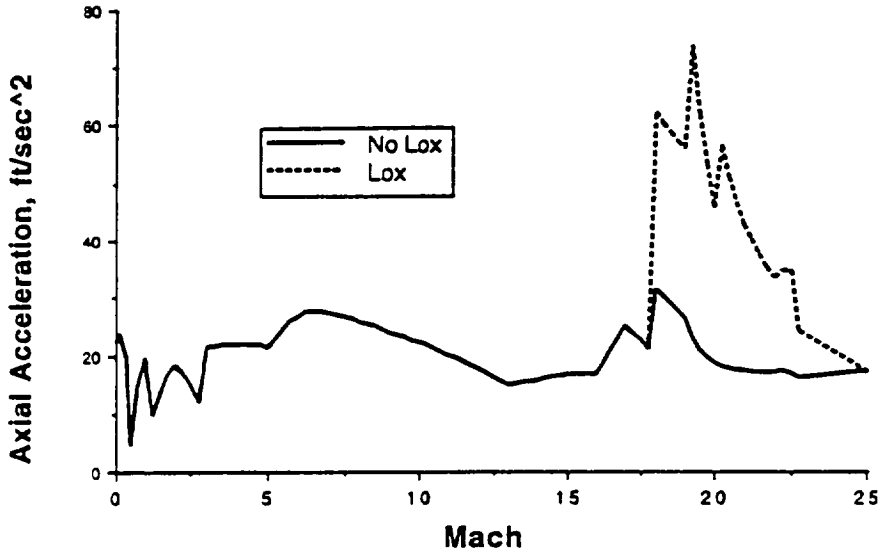

Figure 7. Axial Acceleration

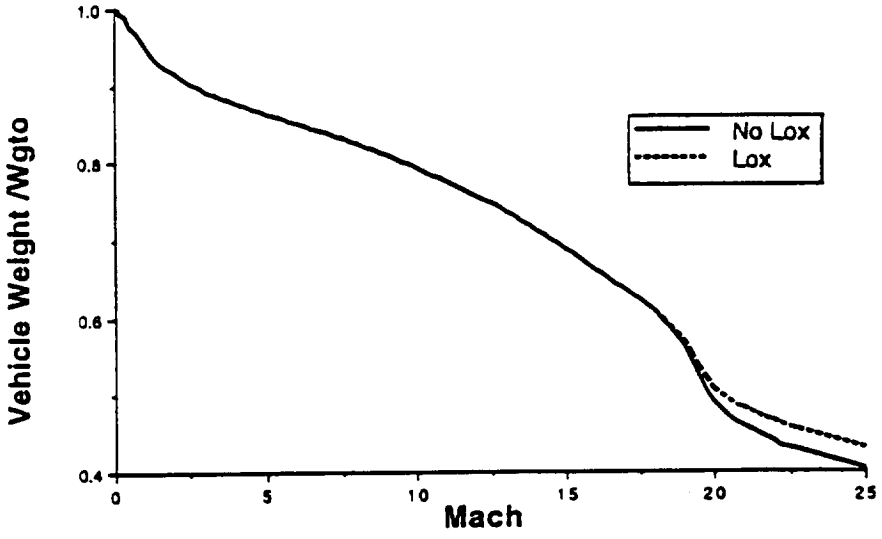

Figure 8. Vehicle Weight With and Without LOX Augmentation

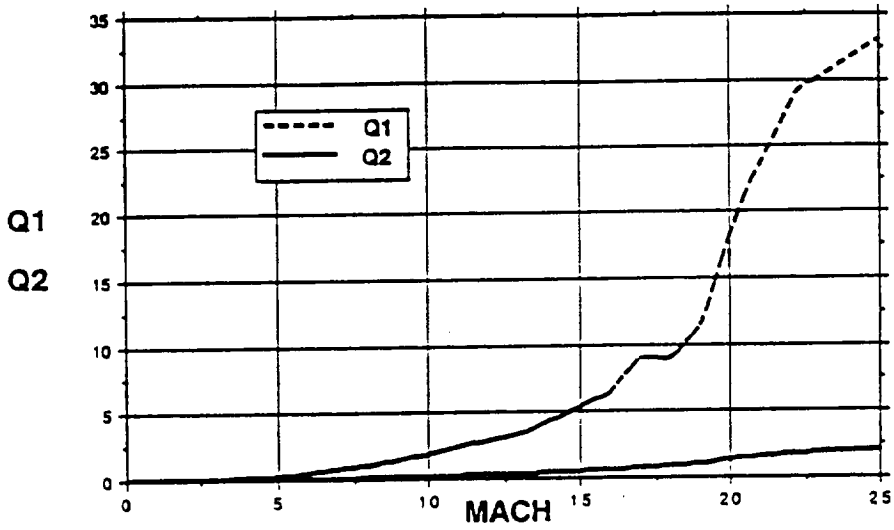

Figure 9. LOX Storage and LOX Collection Optimization Functions

Appendix B

Near-Optimal Operation of Dual-Fuel Launch Vehicles
Submitted to *Journal of Spacecraft and Rockets*

Near-Optimal Operation of Dual-Fuel Launch Vehicles

M. D. Ardema* and H.-C. Chou†
Santa Clara University
Santa Clara, California 95053

and

J.V. Bowles‡
NASA Ames Research Center
Moffett Field, California 94035

Nomenclature

D = drag, lb
E = total mechanical energy per unit weight, ft
g = gravitational acceleration on the earth surface, ft/sec^2
h = altitude, ft
I_{SP} = specific impulse, sec
K = weighting parameter, lb/ft^3
K^* = value of K for minimum empty weight, lb/ft^3
L = lift, lb
LH_2 = liquid hydrogen
M = Mach number
M_{tr} = transition Mach number
M_{tr}^* = optimal transition Mach number
R = radius of the earth, ft
T = thrust, lb
T_V = magnitude of thrust component along velocity vector, lb
t = time, sec
V = speed, fps
v_P = propellant volume, ft^3
W = aircraft earth surface weight (mass), lb
W_P = propellant earth surface weight, lb
ϕ = cost functional
η_{HR} = mass flow ratio of liquid hydrogen to liquid hydrocarbon
η_{OH} = mass flow ratio of liquid oxygen to liquid hydrogen
η_{OR} = mass flow ratio of liquid oxygen to liquid hydrocarbon
ρ = net propellant density, lb/ft^3

Subscripts

DF = dual-fuel mode
E = empty
f = final value
H = liquid hydrogen
LO = lift-off
O = liquid oxygen
R = liquid hydrocarbon

---

* Professor and Chairman, Department of Mechanical Engineering. Associate Fellow AIAA.
† Graduate Research Assistant, Department of Mechanical Engineering. Student Member AIAA.
‡ Aerospace Engineer, System Analysis Branch. Member AIAA.

SF = single-fuel mode
0 = initial value

Introduction

Current studies of single-stage-to-orbit (SSTO) launch vehicles are focused on all-rocket propulsion systems[1,2]. One option for such vehicles is the use of dual-fuel (liquid hydrocarbon and liquid hydrogen (LH_2)), for a portion of the mission[3-6]. As compared with LH_2, hydrocarbon fuel has higher density and produces higher thrust-to-weight, but has lower specific impulse. The advantages of hydrocarbon fuel are important early in the ascent trajectory, and its use may be expected to lead to reduced vehicle size and weight. Because LH_2 is also needed for cooling purposes, in the early portion of the trajectory both fuels must be burned simultaneously. Later in the ascent, when vehicle weight is lower, specific impulse is the key parameter, indicating single-fuel LH_2 use.

Two recent papers[5,6] have considered the optimization of dual-fuel SSTO vehicles. Included was a determination of M_{tr}^*, the Mach Number at which to transition from dual-fuel mode to LH_2 operation in order to minimize vehicle empty weight. Both of these references treat M_{tr} as an external design variable.

In this paper, a guidance algorithm is developed that determines whether dual-fuel or single-fuel operation is superior as an integral part of the trajectory integration. This approach saves a substantial amount of computer time by reducing the number of design variables, and hence the number of design iterations required in a vehicle optimization study. Further, the algorithm will be directly useable in a real-time, on-board, propulsion control system.

The basis of the guidance law is the energy-state dynamic model. The key idea is to introduce the total mechanical energy as a state variable, and then to neglect all other dynamics. When flight path optimization is done with this model, simple rules for the optimal path and for the optimal operation of the propulsion system are obtained. This dynamic model has been used successfully many times to obtain effective guidance laws for a wide variety of aircraft and missions (see Ref. 7 and the references therein for a review of this work). The energy-state approach is particularly suitable for launch vehicles because efficient energy accumulation (or equivalently minimizing "total ΔV") is the primary trajectory optimization goal.

In a series of papers[7-9] we have used energy-state methods to develop algorithms for ascent trajectory optimization and optimal operation of single-fuel multi-mode propulsion systems. In particular, the operation of propulsion systems with two separate engines, air-breathing and rocket, was investigated in Ref. 9. The present paper extends those methods to the dual-fuel case. The main goal is to determine M_v^*, but optimal trajectories are also investigated.

In the numerical results, vehicle performance is computed using the NASA Ames hypersonic vehicle synthesis code (HAVOC), described in Ref. 10. HAVOC integrates geometry, aerodynamics, propulsion, structures, weights, and other computations to produce point designs for a wide variety of launch vehicles. It is capable of iteratively determining "closed" vehicles , that is, designs which meet specified payload mass and volume requirements for a specified mission. Although the trajectory guidance law is based on the energy-state model, the trajectory integration in HAVOC uses a point mass model, including the effects of earth rotation, earth curvature, and variable gravity.

Optimization Function

The energy-state model is obtained by using the total mechanical energy per unit weight as a state variable and then neglecting all the other dynamics. The result is

$$\dot{E} = P \tag{1}$$

$$\dot{W} = -\frac{T}{I_{SP}} \tag{2}$$

where

$$E = \frac{hR}{R+h} + \frac{1}{2g}V^2 \tag{3}$$

and

$$P = \frac{V}{W}(T_v - D) \tag{4}$$

For a SSTO mission, what is desired is a trajectory that gives the minimum empty weight vehicle to put a given payload mass and volume in orbit. Because the density of liquid hydrogen is low, the sensitivity of perturbations in volume need to be taken into consideration as well as mass sensitivity, and it is therefore necessary to minimize a weighted sum of propellant weight and volume. Thus we introduce the cost functional

$$\phi = W_p + K v_p \tag{5}$$

where $K \in [0,\infty)$ is a weighting parameter to be chosen later.

The quantity to be minimized for a given energy gain is

$$J' = \int_{\phi_0}^{\phi_f} d\phi = \int_{t_0}^{t_f} \dot{\phi}\, dt = \int_{E_0}^{E_f} \frac{\dot{\phi}}{P} dE \tag{6}$$

where Eqn. (1) was used. It is assumed that $\dot{\phi} > 0$, $P > 0$ and that E is monotonically increasing. If the propellant density is $\rho = W_p / v_p$, then from Eqns. (2) and (5), and using $\dot{W}_p = -\dot{W}$,

$$\dot{\phi} = \dot{W}_p + K\frac{\dot{W}_p}{\rho} = \frac{T}{I_{SP}}\left(1 + \frac{K}{\rho}\right) \tag{7}$$

For convenience, we choose to invert the integrand in Eqn. (6) and maximize; from Eqns. (1), (6), and (7), the quantity to be maximized is

$$J = \int_{E_0}^{E_f} F dE \tag{8}$$

where

$$F = \frac{V I_{SP}\left(T_V - D\right)}{W T\left(1 + \frac{K}{\rho}\right)} \tag{9}$$

The guidance algorithm then consists of selecting propulsion system and trajectory parameters that maximize the function F as given by Eqn. (9) at each energy level along the trajectory, subject to any relevant constraints.

For vehicles capable of either dual- or single-fuel operation, the densities to be used in Eqn. (9) are

$$\rho_{DF} = \frac{\rho_R \rho_O \rho_H \left(1+\eta_{OR}+\eta_{HR}\right)}{\left(\rho_O \rho_H + \eta_{OR}\rho_R \rho_H + \eta_{HR}\rho_R \rho_O\right)} \tag{10}$$

$$\rho_{SF} = \frac{\rho_O \rho_H \left(1+\eta_{OH}\right)}{\left(\rho_O + \eta_{OH}\rho_H\right)} \tag{11}$$

SSTO vehicles are typically subject to dynamic pressure constraints and a maximum tangential acceleration limit. This latter limit, nominally 3 times the earth surface gravitational acceleration, is met by engine throttling. It may happen that the limit affects dual-fuel operation but not single-fuel operation at a point along the trajectory. All these constraints are accounted for in the guidance algorithm.

Numerical Results

All numerical examples will be based on an SSTO rocket with a delta winged-body configuration[2]. The three propellants (hydrocarbon fuel, LH_2, and liquid oxygen) are stored in three separate internal tanks. The vehicle takes off vertically and lands horizontally. The first results to be presented use a fixed trajectory commonly used for SSTO rockets.

As a first step, the best transition Mach Number, M_{tr}^*, will be determined by treating this parameter as a single external design variable. The results are shown in Figure 1, which plots gross lift-off weight (W_{LO}) and empty weight (W_E) as a function of M_{tr}. It is seen that both minimum W_{LO} and W_E are obtained at about $M_{tr}^* = 9.0$, and that the weight savings at M_{tr}^* are substantial relative to low values of M_{tr}. All of the data points on Figure 1 are for closed vehicles and hence several design iterations are necessary for each point.

Before applying the developed guidance law to this problem, the best value of K must be determined. This is done by computing closed vehicles for a range of values of K (Fig. 2). It is evident that a value of $K = 4$ lb/ft^3, denoted hereafter by K^*, gives very nearly a minimum of both empty weight and gross lift-off weight, and this value will be used throughout the rest of the paper. This value of K^* represents a factor of over 10 in weighting the cost functional in favor of propellant mass (a value of $K = \rho$ would signify equal weighting of propellant mass and volume.) The Figure shows that the use of the optimally weighted cost functional saves 1.7% in empty weight and 1% in gross lift-off weight, relative to minimizing propellant weight only.

It is of interest to compare these results with the equivalent results for an air-breathing launch vehicle, as shown in Figure 2 of Ref. 9. For the airbreather, the best value of K is also around 4, but the empty weight reduction relative to minimizing propellant weight only is much larger, at 4.9%; this is of course because all of the airbreather propellant is low-density LH_2, and therefore this vehicle is more sensitive to volume perturbations.

Figure 3 plots the function F along the fixed trajectory. Whichever mode of operation, dual-fuel or single-fuel, that gives the highest value of F at a given speed should be the one selected at that speed. The figure shows that from lift-off to $M = 9.0$, the dual-fuel mode is superior, and above this speed the single-fuel mode is best. This value of $M_{tr}^* = 9.0$ agrees with the value determined by treating M_{tr} as a design variable, Figure 1, thus validating the guidance law. The value of M_{tr}^* as determined in Refs. 5 was in the range 8.6 - 8.9, and for Ref. 6 it was in the range 7.3 - 7.4.

The relative distance between the two curves on Figure 3 provides an assessment of the difference in performance between the two modes at a given Mach number. It is seen that both modes give substantially the same performance between $M = 7$ and $M = 11$. This relative insensitivity to M_{tr}, characteristic of a design variable near its optimal value, was also observed in Ref. 5. The use of single fuel LH_2 mode becomes increasingly advantageous as Mach number increases past 11.

The function F was also used to optimize the ascent trajectory (Fig. 4). As compared with the fixed trajectory, the near-optimal one has increased dynamic pressure, especially in the initial dual-fuel mode. The plot of F for the two modes along the optimal trajectory is very similar to Fig. 3, except that M_{tr}^* is now 9.6. The near-optimal trajectory consumed less fuel in the amount of 0.9% of W_{LO} than did the fixed, almost all the difference occurring in dual-fuel mode.

Concluding Remarks

A simple guidance law for operation of dual-fuel SSTO launch vehicles has been developed and used to determine the optimal value of the transition Mach Number from dual-fuel to single-fuel. For the example

considered, the optimal transition Mach Number was 9.0 along a fixed trajectory. Along an optimal trajectory, the best transition Mach number was 9.6; the optimal trajectory had higher dynamic pressure than the fixed, particularly in dual-fuel mode.

In the future, the guidance method described in this paper easily could be extended to optimize other propulsion system parameters, such as flow rates of individual propellants in multi-propellant engines. In addition to being a useful tool for preliminary design studies, the guidance law could be used for real-time on-board control of SSTO launch vehicles.

Acknowledgment

This work was supported by NASA Ames Research Center Grant NCC 2-5069.

References

[1]Bekey, I., "SSTO Rockets; A practical Possibility," *Aerospace America*, July 1994, pp. 32-37.

[2]Freeman, D. C., Talay, T. A.,Stanley, D. O., Lepsch, R. A., and Wilhite, A. W., "Design Options for Advanced Manned Launch Systems," *Journal of Spacecraft and Rockets*, Vol. 32, No. 2, March-April 1995, pp. 241-249.

[3]Salkeld, R., "Mixed-Mode Propulsion for the Space Shuttle," *Astronautics and Aeronautics*, Vol. 9, No. 8, 1971, pp. 52-58.

[4]Wilhite, A. W., "Optimization of Rocket Propulsion Systems for Advanced Earth-to-Orbit Shuttles," *Journal of Spacecraft and Rockets*, Vol. 17, No. 2, 1980, pp. 99-104.

[5]Lepsch, R. A., Stanley, D. O., and Unal, R., "Dual-Fuel Propulsion in Single-State Advanced Manned Launch System Vehicle," *Journal of Spacecraft and Rockets*, Vol. 32, No. 3, May-June 1995, pp. 417-425.

[6]Braun, R. D., Powel, R. W., Lepsch, R. A., Stanley, D. O., and Kroo, I. M., "Comparison of Two Multidisciplinary Optimization Strategies for Launch-Vehicle Design," *Journal of Spacecraft and Rockets*, Vol. 32, No. 3, May-June 1995, pp. 404-410.

[7]Ardema, M. D., Bowles, J. V., and Whittaker, T., "Optimal Trajectories for Hypersonic Launch Vehicles," *Dynamics and Control*, 4, 1994, pp. 337-347.

[8]Ardema, M. D., Bowles, J. V., Terjesen, E. J., and Whittaker, T., "Approximate Altitude Transitions for High-Speed Aircraft," *Journal of Guidance, Control, and Dynamics*, Vol. 18, No. 3, May-June 1995, pp. 561-566.

[9]Ardema, M. D., Bowles, J. V., and Whittaker, T., "Near-Optimal Propulsion System Operation for Air-Breathing Launch Vehicles," *Proceedings of the 1994 AIAA Guidance, Navigation, and Control Conf.*, Scottsdale, AZ, Aug. 1-3, 1994.

[10]Bowles, J. V., "Ames Conceptual Studies Activities," *Proceedings of the Second National Aerospace Plane Symposium*, Applied Physics Lab., Laurel, MD, Nov. 1986.

List of Figures

Figure 1. Effect of transition Mach number on vehicle gross lift-off weight and empty weight.

Figure 2. Variation of gross lift-off weight and empty weight with weighting parameter K.

Figure 3. Cost functional histories for dual- and single-fuel propulsion modes.

Figure 4. The fixed and optimized flight paths.

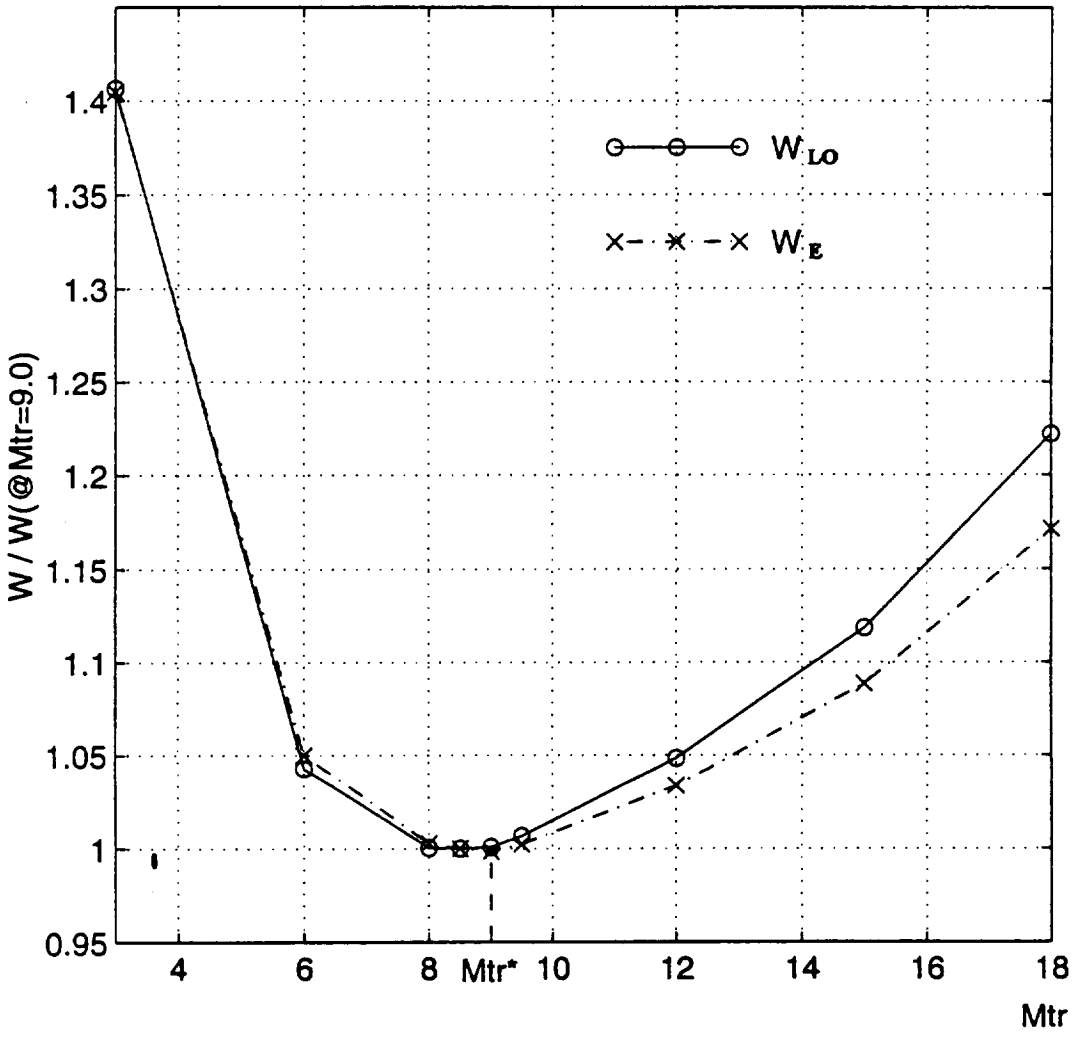

Figure 1. Effect of transition Mach number on vehicle gross lift-off weight and empty weight.

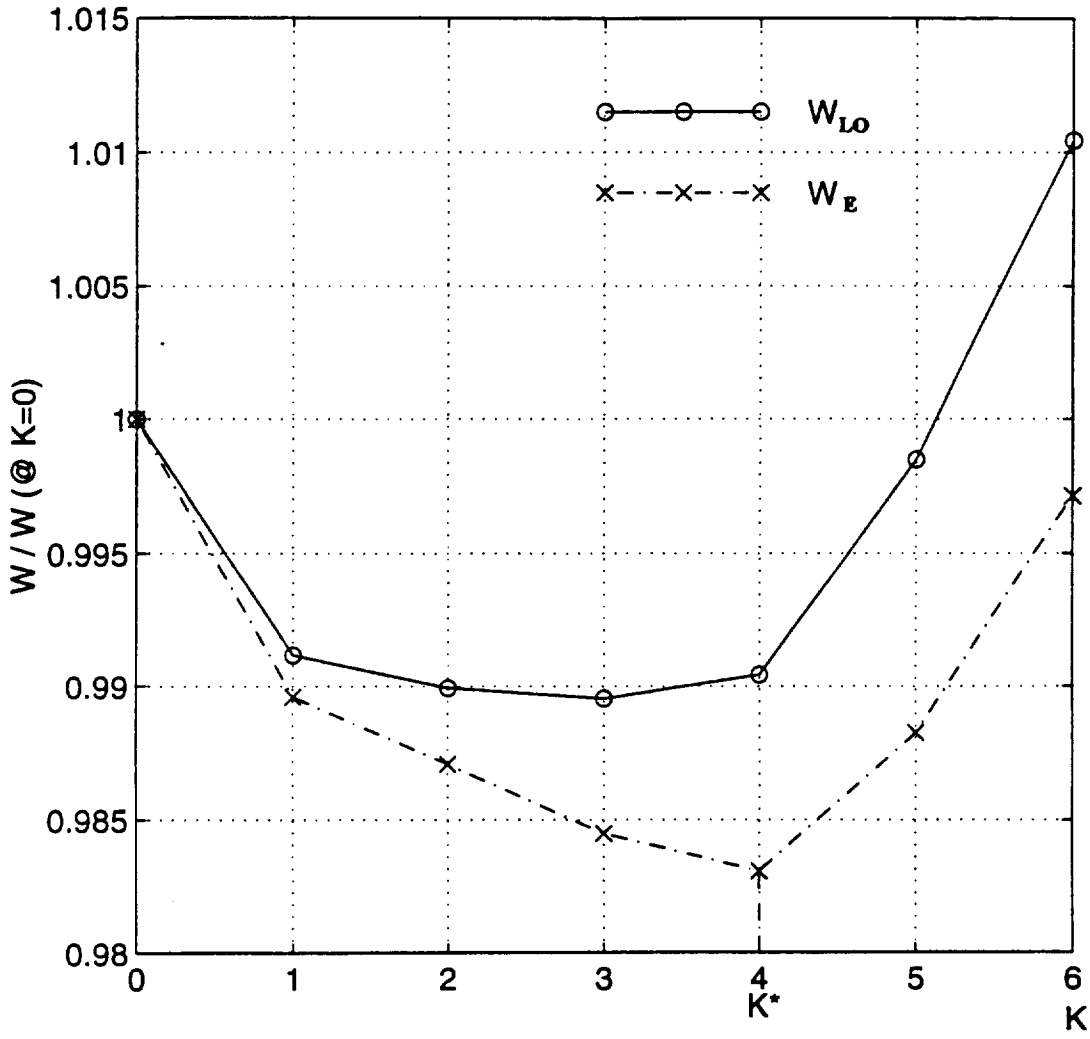

Figure 2. Variation of gross lift-off weight and empty weight with weighting parameter *K*.

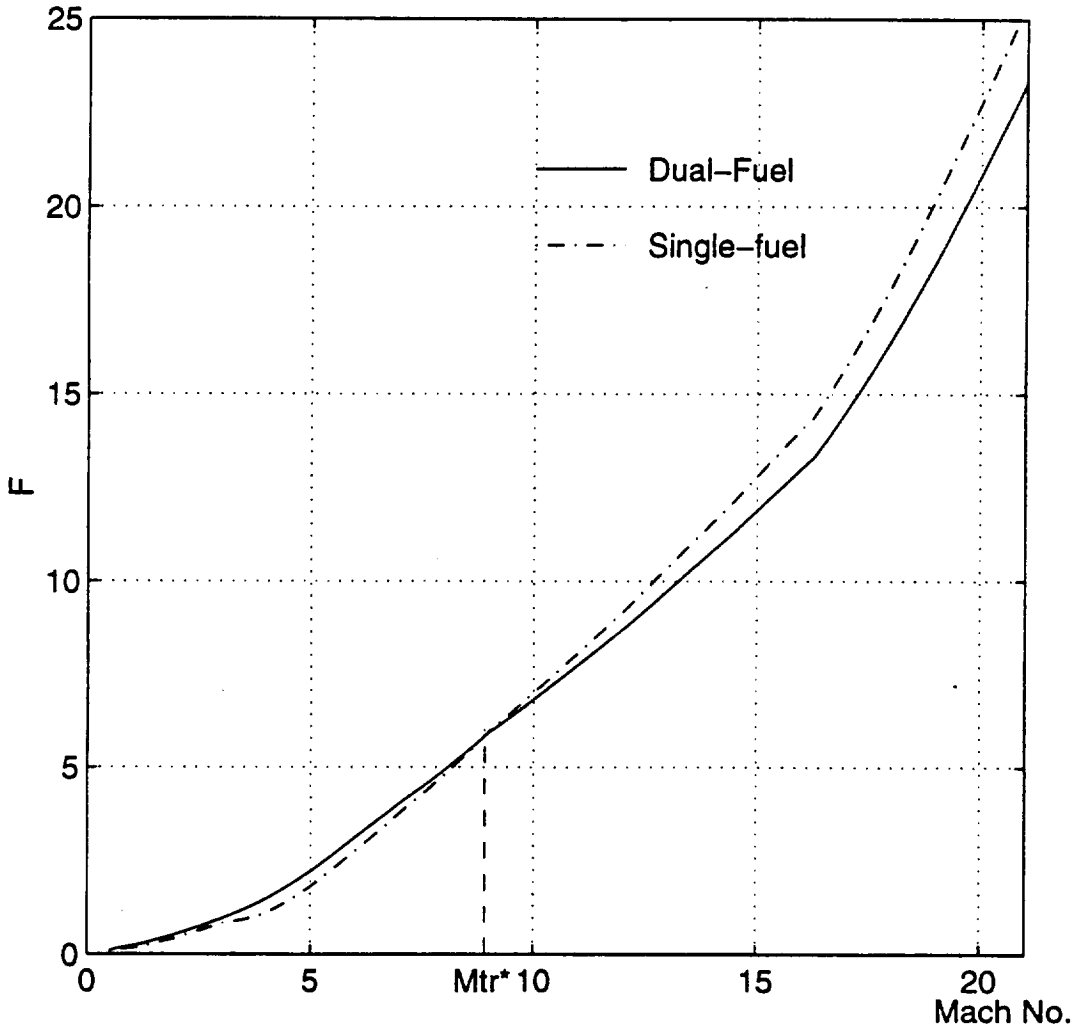

Figure 3. Cost functional histories for dual- and single-fuel propulsion modes.

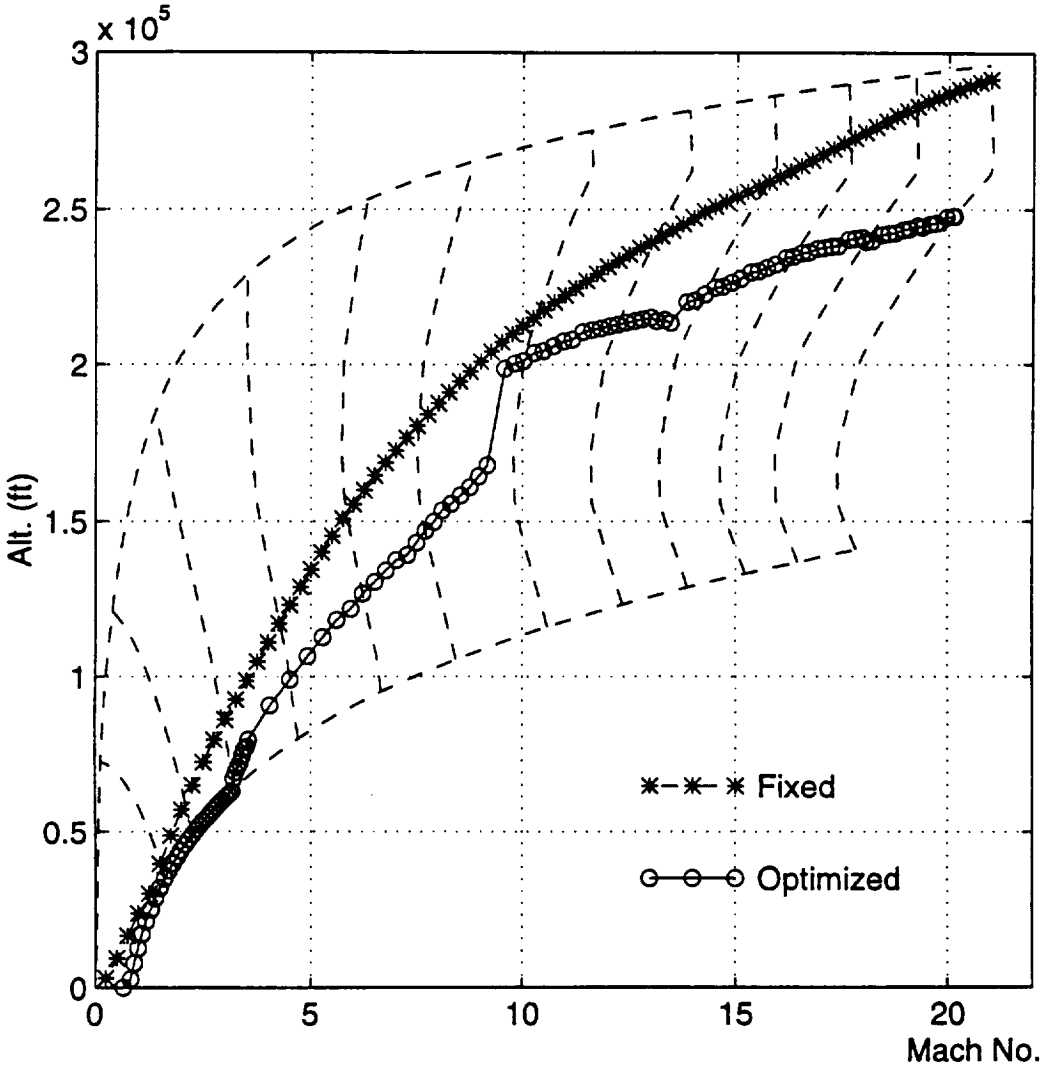

Figure 4. The fixed and optimized flight paths.